

RMPflow: A Computational Graph for Automatic Motion Policy Generation

Ching-An Cheng^{1,2}, Mustafa Mukadam^{1,2}, Jan Issac¹, Stan Birchfield¹,
Dieter Fox^{1,3}, Byron Boots^{1,2}, and Nathan Ratliff¹

¹ NVIDIA, Seattle Robotics Lab, Seattle, WA, USA

² Georgia Institute of Technology, Robot Learning Lab, Atlanta, GA, USA

³ University of Washington, Robotics and State Estimation Lab, Seattle, WA, USA

Abstract. We develop a novel policy synthesis algorithm, RMPflow, based on geometrically consistent transformations of Riemannian Motion Policies (RMPs). RMPs are a class of reactive motion policies designed to parameterize non-Euclidean behaviors as dynamical systems in intrinsically nonlinear task spaces. Given a set of RMPs designed for individual tasks, RMPflow can consistently combine these local policies to generate an expressive global policy, while simultaneously exploiting sparse structure for computational efficiency. We study the geometric properties of RMPflow and provide sufficient conditions for stability. Finally, we experimentally demonstrate that accounting for the geometry of task policies can simplify classically difficult problems, such as planning through clutter on high-DOF manipulation systems.

Keywords: Motion and Path Planning, Collision Avoidance, Dynamics

1 Introduction

In this work, we develop a new motion generation and control framework that enables globally stable controller design within *intrinsically* non-Euclidean spaces.⁴ Non-Euclidean geometries are not often modeled explicitly in robotics, but are nonetheless common in the natural world. One important example is the apparent non-Euclidean behavior of obstacle avoidance. Obstacles become holes in this setting. As a result, straight lines are no longer a reasonable definition of shortest distance—geodesics must, therefore, naturally flow around them. This behavior implies a form of non-Euclidean geometry: the space is naturally curved by the presence of obstacles.

The planning literature has made substantial progress in modeling non-Euclidean task-space behaviors, but at the expense of efficiency and reactivity. Starting with early differential geometric models of obstacle avoidance [1] and building toward modern planning algorithms and optimization techniques [2–9], these techniques can calculate highly nonlinear trajectories. However, they are often computationally intensive, sensitive to noise, and unresponsive to perturbation. In addition, the internal nonlinearities of robots due to kinematic constraints are sometimes simplified in the optimization.

⁴ Spaces defined by non-constant Riemannian metrics with non-trivial curvature.

At the same time, a separate thread of literature, emphasizing fast reactive control over computationally expensive planning, developed efficient closed-loop control techniques such as Operational Space Control (OSC) [10]. But while these techniques account for internal geometries from the robot’s kinematic structure, they assume simple Euclidean geometry in task spaces [11, 12], failing to provide a complete treatment of the external geometries. As a result, obstacle avoidance, e.g., has to rely on *extrinsic* potential functions, leading to undesirable deacceleration behavior when the robot is close to the obstacle. If the non-Euclidean geometry can be *intrinsically* considered, then fast obstacle avoidance motion would naturally arise as traveling along the induced geodesic. The need for a holistic solution to motion generation and control has motivated a number of recent system architectures tightly integrating planning and control [13, 14].

We develop a new approach to synthesizing control policies that can accommodate and leverage the modeling capacity of intrinsically non-Euclidean robotics tasks. Taking inspiration from Geometric Control Theory [15],⁵ we design a novel recursive algorithm, RMPflow, based on a recently proposed mathematical object for representing nonlinear policies known as the Riemannian Motion Policy (RMP) [16]. This algorithm enables the geometrically consistent fusion of many component policies defined across non-Euclidean task spaces that are related through a tree structure. We show that RMPflow, which generates behavior by calculating how the robot should accelerate, mimics the Recursive Newton-Euler algorithm [17] in structure, but generalizes it beyond rigid-body systems to a broader class of highly-nonlinear transformations and spaces.

In contrast to existing frameworks, our framework naturally models non-Euclidean task spaces with Riemannian metrics that are not only configuration dependent, but also *velocity* dependent. This allows RMPflow to consider, e.g., the *direction* a robot travels to define the importance weights in combining policies. For example, an obstacle, despite being close to the robot, can usually be ignored if robot is heading away from it. This new class of policies leads to an extension of Geometric Control Theory, building on a new class of non-physical mechanical systems we call Geometric Dynamical Systems (GDS).

We also show that RMPflow is Lyapunov-stable and coordinate-free. In particular, when using RMPflow, robots can be viewed each as different parameterizations of the same task space, defining a precise notion of behavioral consistency between robots. Additionally, under this framework, the implicit curvature arising from non-constant Riemannian metrics (which may be roughly viewed as position-velocity dependent inertia matrices in OSC) produces nontrivial and intuitive policy contributions that are critical to guaranteeing stability and generalization across embodiments. Our experimental results illustrate how these curvature terms can be impactful in practice, generating nonlinear geodesics that result in curving or orbiting around obstacles. Finally, we demonstrate the utility of our framework with a fully reactive real-world system on multiple dual-arm manipulation problems.

⁵ See Appendix A.1 for a discussion of why geometric mechanics and geometric control theory constitute a good starting point.

2 Motion Generation and Control

Motion generation and control can be formulated as the problem of transforming curves from the configuration space \mathcal{C} to the task space \mathcal{T} . Specifically, let \mathcal{C} be a d -dimensional smooth manifold. A robot’s motion can be described as a curve $q : [0, \infty) \rightarrow \mathcal{C}$ such that the robot’s configuration at time t is a point $q(t) \in \mathcal{C}$. Without loss of generality, suppose \mathcal{C} has a global coordinate $\mathbf{q} : \mathcal{C} \rightarrow \mathbb{R}^d$, called the *generalized coordinate*; for short, we would identify the curve q with its coordinate and write $\mathbf{q}(q(t))$ as $\mathbf{q}(t) \in \mathbb{R}^d$. A typical example of the generalized coordinate is the joint angles of a d -DOF (degrees-of-freedom) robot: we denote $\mathbf{q}(t)$ as the joint angles at time t and $\dot{\mathbf{q}}(t)$, $\ddot{\mathbf{q}}(t)$ as the joint velocities and accelerations. To describe the tasks, we consider another manifold \mathcal{T} , the task space, which is related to the configuration space \mathcal{C} through a smooth *task map* $\psi : \mathcal{C} \rightarrow \mathcal{T}$. The task space \mathcal{T} can be the end-effector position/orientation [10, 18], or more generally can be a space that describes whole-body robot motion, e.g., in simultaneous tracking and collision avoidance [19, 20]. Thus, the goal of motion generation and control is to design the curve q so that the transformed curve $\psi \circ q$ exhibits desired behaviors on the task space \mathcal{T} .

Notation For clarity, we use boldface to distinguish the coordinate-dependent representations from abstract objects; e.g. we write $q(t) \in \mathcal{C}$ and $\mathbf{q}(t) \in \mathbb{R}^d$. In addition, we will often omit the time- and input-dependency of objects unless necessary; e.g. we may write $q \in \mathcal{C}$ and $(\mathbf{q}, \dot{\mathbf{q}}, \ddot{\mathbf{q}})$. For derivatives, we use both symbols ∇ and ∂ , with a transpose relationship: for $\mathbf{x} \in \mathbb{R}^m$ and a differential map $\mathbf{y} : \mathbb{R}^m \rightarrow \mathbb{R}^n$, we write $\nabla_{\mathbf{x}}\mathbf{y}(\mathbf{x}) = \partial_{\mathbf{x}}\mathbf{y}(\mathbf{x})^\top \in \mathbb{R}^{m \times n}$. For a matrix $\mathbf{M} \in \mathbb{R}^{m \times m}$, we denote $\mathbf{m}_i = (\mathbf{M})_i$ as its i th column and $M_{ij} = (\mathbf{M})_{ij}$ as its (i, j) element. To compose a matrix, we use $(\cdot)^\top$ for vertical (or matrix) concatenation and $[\cdot]$ for horizontal concatenation. For example, we write $\mathbf{M} = [\mathbf{m}_i]_{i=1}^m = (M_{ij})_{i,j=1}^m$ and $\mathbf{M}^\top = (\mathbf{m}_i^\top)_{i=1}^m = (M_{ji})_{i,j=1}^m$. We use $\mathbb{R}_+^{m \times m}$ and $\mathbb{R}_{++}^{m \times m}$ to denote the symmetric, positive semi-definite/definite matrices, respectively.

2.1 Motion Policies and the Geometry of Motion

We model motion as a second-order differential equation⁶ of $\ddot{\mathbf{q}} = \pi(\mathbf{q}, \dot{\mathbf{q}})$, where we call π a *motion policy* and $(\mathbf{q}, \dot{\mathbf{q}})$ the *state*. In contrast to an open-loop trajectory, which forms the basis of many motion planners, a motion policy expresses the entire continuous collection of its integral trajectories and therefore is robust to perturbations. Motion policies can model many adaptive behaviors, such as reactive obstacle avoidance [21, 13] or responses driven by planned Q-functions [22], and their second-order formulation enables rich behavior that cannot be realized by the velocity-based approach [23].

The geometry of motion has been considered by many planning and control algorithms. Geometrical modeling of task spaces is used in topological motion planning [3], and motion optimization has leveraged Hessian to exploit the natural geometry of costs [24, 5, 25, 26]. Ratliff et al. [2], e.g., use the workspace ge-

⁶ We assume the system has been feedback linearized. A torque-based setup can be similarly derived by setting the robot inertia matrix as the intrinsic metric on \mathcal{C} [11].

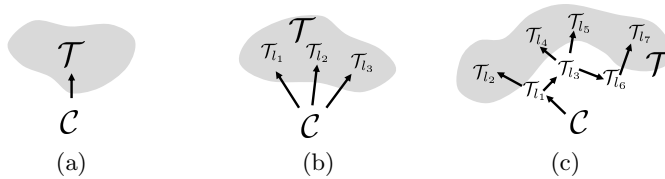


Fig. 1: Tree-structured task maps

ometry inside a Gauss-Newton optimizer and generate natural obstacle-avoiding reaching motion through traveling along geodesics of curved spaces.

Geometry-aware motion policies were also developed in parallel in controls. OSC is the best example [10]. Unlike the planning approaches, OSC focuses on the internal geometry of the robot and considers only simple task-space geometry. It reshapes the workspace dynamics into a simple spring-mass-damper system with a constant inertia matrix, enforcing a form of Euclidean geometry in the task space. Variants of OSC have been proposed to consider different metrics [27, 11, 20], task hierarchies [19, 28], and non-stationary inputs [29].

While these algorithms have led to many advances, we argue that their isolated focus on either the internal or the external geometry limits the performance. The planning approach fails to consider reactive dynamic behavior; the control approach cannot model the effects of velocity dependent metrics, which are critical to generating sensible obstacle avoidance motions, as discussed in the introduction. While the benefits of velocity dependent metrics was recently explored using RMPs [16], a systematic understanding is still an open question.

3 Automatic Motion Policy Generation with RMPflow

RMPflow is an efficient manifold-oriented computational graph for automatic generation of motion policies. It is aimed for problems with a task space $\mathcal{T} = \{\mathcal{T}_i\}$ that is related to the configuration space \mathcal{C} through a tree-structured task map ψ , where \mathcal{T}_i is the i th subtask. Given user-specified motion policies $\{\pi_{i_i}\}$ on $\{\mathcal{T}_i\}$ as RMPs, RMPflow is designed to *consistently* combine these subtask policies into a global policy π on \mathcal{C} . To this end, RMPflow introduces 1) a data structure, called the *RMP-tree*, to describe the tree-structured task map ψ and the policies, and 2) a set of operators, called the *RMP-algebra*, to propagate information across the RMP-tree. To compute $\pi(\mathbf{q}(t), \dot{\mathbf{q}}(t))$ at time t , RMPflow operates in two steps: it first performs a *forward pass* to propagate the state from the root node (i.e. \mathcal{C}) to the leaf nodes (i.e. $\{\mathcal{T}_i\}$); then it performs a *backward pass* to propagate the RMPs from the leaf nodes to the root node. These two steps are realized by recursive use of RMP-algebra, exploiting shared computation paths arising from the tree structure to maximize efficiency.

3.1 Structured Task Maps

In most cases, the task-space manifold \mathcal{T} is structured. In this paper, we consider the case where the task map ψ can be expressed through a tree-structured composition of transformations $\{\psi_{e_i}\}$, where ψ_{e_i} is the i th transformation. Fig. 1 illustrates some common examples. Each node denotes a manifold and each edge

denotes a transformation. This family trivially includes the unstructured task space \mathcal{T} (Fig. 1a) and the product manifold $\mathcal{T} = \mathcal{T}_{l_1} \times \cdots \times \mathcal{T}_{l_K}$ (Fig. 1b), where K is the number of subtasks. A more interesting example is the kinematic tree (Fig. 1c), where, e.g., the subtask spaces on the leaf nodes can describe the tracking and obstacle avoidance tasks along a multi-DOF robot.

The main motivation of explicitly handling the structure in the task map ψ is two-fold. First, it allows RMPflow to exploit computation shared across different subtask maps. Second, it allows the user to focus on designing motion policies for each subtask individually, which is easier than directly designing a global policy for the entire task space \mathcal{T} . For example, \mathcal{T} may describe the problem of humanoid walking, which includes staying balanced, scheduling contacts, and avoiding collisions. Directly parameterizing a policy to satisfy all these objectives can be daunting, whereas designing a policy for each subtask is more feasible.

3.2 Riemannian Motion Policies (RMPs)

Knowing the structure of the task map is not sufficient for consistently combining subtask policies: we require some geometric information about the motion policies' behaviors [16]. Toward this end, we adopt an abstract description of motion policies, called RMPs [16], for the nodes of the RMP-tree. Specifically, let \mathcal{M} be an m -dimensional manifold with coordinate $\mathbf{x} \in \mathbb{R}^m$. The *canonical form* of an RMP on \mathcal{M} is a pair $(\mathbf{a}, \mathbf{M})^{\mathcal{M}}$, where $\mathbf{a} : \mathbb{R}^m \times \mathbb{R}^m \rightarrow \mathbb{R}^m$ is a continuous motion policy and $\mathbf{M} : \mathbb{R}^m \times \mathbb{R}^m \rightarrow \mathbb{R}_+^{m \times m}$ is a differentiable map. Borrowing terminology from mechanics, we call $\mathbf{a}(\mathbf{x}, \dot{\mathbf{x}})$ the *desired acceleration* and $\mathbf{M}(\mathbf{x}, \dot{\mathbf{x}})$ the *inertia matrix* at $(\mathbf{x}, \dot{\mathbf{x}})$, respectively.⁷ \mathbf{M} defines the directional importance of \mathbf{a} when it is combined with other motion policies. Later in Section 4, we will show that \mathbf{M} is closely related to Riemannian metric, which describes how the space is stretched along the curve generated by \mathbf{a} ; when \mathbf{M} depends on the state, the space becomes *non-Euclidean*. We additionally introduce a new RMP form, called the *natural form*. Given an RMP in its canonical form $(\mathbf{a}, \mathbf{M})^{\mathcal{M}}$, the natural form is a pair $[\mathbf{f}, \mathbf{M}]^{\mathcal{M}}$, where $\mathbf{f} = \mathbf{M}\mathbf{a}$ is the *desired force* map. While the transformation between these two forms may look trivial, their distinction will be useful later when we introduce the RMP-algebra.

3.3 RMP-tree

The RMP-tree is the core data structure used by RMPflow. An RMP-tree is a directed tree, in which each node represents an RMP and its state, and each edge corresponds to a transformation between manifolds. The root node of the RMP-tree describes the global policy π on \mathcal{C} , and the leaf nodes describe the local policies $\{\pi_{l_i}\}$ on $\{\mathcal{T}_{l_i}\}$. To illustrate, let us consider a node u and its K child nodes $\{v_i\}_{i=1}^K$. Suppose u describes an RMP $[\mathbf{f}, \mathbf{M}]^{\mathcal{M}}$ and v_i describes an RMP $[\mathbf{f}_i, \mathbf{M}_i]^{\mathcal{N}_i}$, where $\mathcal{N}_i = \psi_{e_i}(\mathcal{M})$ for some ψ_{e_i} . Then we write $u = ((\mathbf{x}, \dot{\mathbf{x}}), [\mathbf{f}, \mathbf{M}]^{\mathcal{M}})$ and $v_i = ((\mathbf{y}_i, \dot{\mathbf{y}}_i), [\mathbf{f}_i, \mathbf{M}_i]^{\mathcal{N}_i})$; the edge connecting u and v_i points from u to v_i along ψ_{e_i} . We will continue to use this example to illustrate how RMP-algebra propagates the information across the RMP-tree.

⁷ Here we adopt a slightly different terminology from [16]. We note that \mathbf{M} and \mathbf{f} do not necessarily correspond to the inertia and force of a physical mechanical system.

3.4 RMP-algebra

The RMP-algebra consists of three operators (**pushforward**, **pullback**, and **resolve**) to propagate information.⁸ They form the basis of the forward and backward passes for automatic policy generation, described in the next section.

1. **pushforward** is the operator to forward propagate the *state* from a parent node to its child nodes. Using the previous example, given $(\mathbf{x}, \dot{\mathbf{x}})$ from u , it computes $(\mathbf{y}_i, \dot{\mathbf{y}}_i) = (\psi_{e_i}(\mathbf{x}), \mathbf{J}_i(\mathbf{x})\dot{\mathbf{x}})$ for each child node v_i , where $\mathbf{J}_i = \partial_{\mathbf{x}}\psi_{e_i}$ is a Jacobian matrix. The name “pushforward” comes from the linear transformation of tangent vector $\dot{\mathbf{x}}$ to the image tangent vector $\dot{\mathbf{y}}_i$.
2. **pullback** is the operator to backward propagate the natural-formed RMPs from the child nodes to the parent node. It is done by setting $[\mathbf{f}, \mathbf{M}]^{\mathcal{M}}$ with

$$\mathbf{f} = \sum_{i=1}^K \mathbf{J}_i^{\top} (\mathbf{f}_i - \mathbf{M}_i \dot{\mathbf{J}}_i \dot{\mathbf{x}}) \quad \text{and} \quad \mathbf{M} = \sum_{i=1}^K \mathbf{J}_i^{\top} \mathbf{M}_i \mathbf{J}_i \quad (1)$$

The name “pullback” comes from the linear transformations of the cotangent vector (1-form) $\mathbf{f}_i - \mathbf{M}_i \dot{\mathbf{J}}_i \dot{\mathbf{x}}$ and the inertia matrix (2-form) \mathbf{M}_i . In summary, velocities can be pushforwarded along the direction of ψ_i , and forces and inertial matrices can be pullbacked in the opposite direction.

To gain more intuition of **pullback**, we write **pullback** in the canonical form of RMPs. It can be shown that the canonical form $(\mathbf{a}, \mathbf{M})^{\mathcal{M}}$ of the natural form $[\mathbf{f}, \mathbf{M}]^{\mathcal{M}}$ above is the solution to a least-squared problem:

$$\mathbf{a} = \arg \min_{\mathbf{a}'} \frac{1}{2} \sum_{i=1}^K \|\mathbf{J}_i \mathbf{a}' + \dot{\mathbf{J}}_i \dot{\mathbf{x}} - \mathbf{a}_i\|_{\mathbf{M}_i}^2 \quad (2)$$

where $\mathbf{a}_i = \mathbf{M}_i^{\dagger} \mathbf{f}_i$ and $\|\cdot\|_{\mathbf{M}_i}^2 = \langle \cdot, \mathbf{M}_i \cdot \rangle$. Because $\ddot{\mathbf{y}}_i = \mathbf{J}_i \ddot{\mathbf{x}} + \dot{\mathbf{J}}_i \dot{\mathbf{x}}$, **pullback** attempts to find an \mathbf{a} that can realize the desired accelerations $\{\mathbf{a}_i\}$ while trading off approximation errors with an importance weight defined by the inertia matrix $\mathbf{M}_i(\mathbf{y}_i, \dot{\mathbf{y}}_i)$. The use of state dependent importance weights is a distinctive feature of RMPflow. It allows RMPflow to activate different RMPs according to *both* configuration and velocity (see Section 3.6 for examples). Finally, we note that the **pullback** operator defined in this paper is slightly different from the original definition given in [16], which ignores the term $\dot{\mathbf{J}}_i \dot{\mathbf{x}}$ in (2). While ignoring $\dot{\mathbf{J}}_i \dot{\mathbf{x}}$ does not necessary destabilize the system [20], its inclusion is critical to implement consistent policy behaviors.

3. **resolve** is the last operator of RMP-algebra. It maps an RMP from its natural form to its canonical form. Given $[\mathbf{f}, \mathbf{M}]^{\mathcal{M}}$, it outputs $(\mathbf{a}, \mathbf{M})^{\mathcal{M}}$ with $\mathbf{a} = \mathbf{M}^{\dagger} \mathbf{f}$, where \dagger denotes Moore-Penrose inverse. The use of pseudo-inverse is because in general the inertia matrix is only positive semi-definite. Therefore, we also call the natural form of $[\mathbf{f}, \mathbf{M}]^{\mathcal{M}}$ the *unresolved form*, as potentially it can be realized by multiple RMPs in the canonical form.

3.5 Algorithm: Motion Policy Generation

Now we show how RMPflow uses the RMP-tree and RMP-algebra to generate a global policy π on \mathcal{C} . Suppose each subtask policy is provided as an RMP. First,

⁸ Precisely it propagates the numerical values of RMPs and states at a particular time.

we construct an RMP-tree with the same structure as ψ , where we assign subtask RMPs as the leaf nodes and the global RMP $[\mathbf{f}_r, \mathbf{M}_r]^c$ as the root node. With the RMP-tree specified, RMPflow can perform automatic policy generation. At every time instance, it first performs a forward pass: it recursively calls `pushforward` from the root node to the leaf nodes to update the state information in each node in the RMP-tree. Second, it performs a backward pass: it recursively calls `pullback` from the leaf nodes to the root node to back propagate the values of the RMPs in the natural form, and finally calls `resolve` at the root node to transform the global RMP $[\mathbf{f}_r, \mathbf{M}_r]^c$ into its canonical form $(\mathbf{a}_r, \mathbf{M}_r)^c$ for policy execution (i.e. setting $\pi(\mathbf{q}, \dot{\mathbf{q}}) = \mathbf{a}_r$).

The process of policy generation of RMPflow uses the tree structure for computational efficiency. For K subtasks, it has time complexity $O(K)$ in the worst case as opposed to $O(K \log K)$ of a naive implementation which does not exploit the tree structure. Furthermore, all computations of RMPflow are carried out using matrix-multiplications, except for the final `resolve` call, because the RMPs are expressed in the natural form in `pullback` instead of the canonical form suggested originally in [16]. This design makes RMPflow numerically stable, as only one matrix inversion $\mathbf{M}_r^\dagger \mathbf{f}_r$ is performed at the root node with both \mathbf{f}_r and \mathbf{M}_r in the span of the same Jacobian matrix due to `pullback`.

3.6 Example RMPs

We give a quick overview of some RMPs useful in practice (a complete discussion of these RMPs are postponed to Appendix D). We recall from (2) that \mathbf{M} dictates the directional importance of an RMP.

Collision/joint limit avoidance Barrier-type RMPs are examples that use velocity dependent inertia matrices, which can express importance as a function of robot heading (a property that traditional mechanical principles fail to capture). Here we demonstrate a collision avoidance policy in the 1D distance space $x = d(\mathbf{q})$ to an obstacle. Let $g(x, \dot{x}) = w(x)u(\dot{x}) > 0$ for some functions w and u . We consider a motion policy such that $m(x, \dot{x})\ddot{x} + \frac{1}{2}\dot{x}^2\partial_x g(x, \dot{x}) = -\partial_x \Phi(x) - b\dot{x}$ and define its inertia matrix $m(x, \dot{x}) = g(x, \dot{x}) + \frac{1}{2}\dot{x}\partial_{\dot{x}}g(x, \dot{x})$, where Φ is a potential and $b > 0$ is a damper. We choose $w(x)$ to increase as x decreases (close to the obstacle), $u(\dot{x})$ to increase when $\dot{x} < 0$ (moving toward the obstacle), and $u(\dot{x})$ to be constant when $\dot{x} \geq 0$. With this choice, the RMP can be turned off in `pullback` when the robot heads away from the obstacle. This motion policy is a GDS and g is its metric (cf. Section 4.1); the terms $\frac{1}{2}\dot{x}\partial_{\dot{x}}g(x, \dot{x})$ and $\frac{1}{2}\dot{x}^2\partial_x g(x, \dot{x})$ are due to non-Euclidean geometry and produce natural repulsive behaviors.

Target attractors Designing an attractor policy is relatively straightforward. For a task space with coordinate \mathbf{x} , we can consider an inertia matrix $\mathbf{M}(\mathbf{x}) \succ 0$ and a motion policy such that $\ddot{\mathbf{x}} = -\nabla\tilde{\Phi} - \beta(\mathbf{x})\dot{\mathbf{x}} - \mathbf{M}^{-1}\boldsymbol{\xi}_M$, where $\tilde{\Phi}(\mathbf{x}) \approx \|\mathbf{x}\|$ is a smooth attractor potential, $\beta(\mathbf{x}) \geq 0$ is a damper, and $\boldsymbol{\xi}_M$ is a curvature term. It can be shown that this differential equation is also a GDS (see Appendix D.4).

Orientations As RMPflow directly works with manifold objects, orientation controllers become straightforward to design, independent of the choice of coordinate (cf. Section 4.4). For example, we can define RMPs on a robotic link's

surface in any preferred coordinate (e.g. in one or two axes attached to an arbitrary point) with the above described attractor to control the orientation. This follows a similar idea outlined in the Appendix of [16].

Q-functions Perhaps surprising, RMPs can be constructed using Q-functions as metrics (we invite readers to read [16] for details on how motion optimizers can be reduced to Q-functions and the corresponding RMPs). While these RMPs may not satisfy the conditions of a GDS that we later analyze, they represent a broader class of RMPs that leads to substantial benefits (e.g. escaping local minima) in practice. Also, Q-functions are closely related to Lyapunov functions and geometric control [30]; we will further explore this direction in future work.

4 Theoretical Analysis of RMPflow

We investigate the properties of RMPflow when the child-node motion policies belong to a class of differential equations, which we call *structured geometric dynamical systems* (structured GDSs). We present the following results.

1. **Closure:** We show that the `pullback` operator retains a closure of structured GDSs. When the child-node motion policies are structured GDSs, the parent-node dynamics also belong to the same class.
2. **Stability:** Using the closure property, we provide sufficient conditions for the feedback policy of RMPflow to be stable. In particular, we cover a class of dynamics with *velocity-dependent* metrics that are new to the literature.
3. **Invariance:** As its name suggests, RMPflow is closely related to differential geometry. We show that RMPflow is intrinsically coordinate-free. This means that a set of subtask RMPs designed for one robot can be transferred to another robot while maintaining the same task-space behaviors.

Setup We assume that all manifolds and maps are sufficiently smooth. For now, we also assume that each manifold has a single chart; the coordinate-free analysis is postponed to Section 4.4. All the proofs are provided in Appendix B.

4.1 Geometric Dynamical Systems (GDSs)

We define a new family of dynamics useful to specify RMPs on manifolds. Let manifold \mathcal{M} be m -dimensional with chart $(\mathcal{M}, \mathbf{x})$. Let $\mathbf{G} : \mathbb{R}^m \times \mathbb{R}^m \rightarrow \mathbb{R}_+^{m \times m}$, $\mathbf{B} : \mathbb{R}^m \times \mathbb{R}^m \rightarrow \mathbb{R}_+^{m \times m}$, and $\Phi : \mathbb{R}^m \rightarrow \mathbb{R}$. The tuple $(\mathcal{M}, \mathbf{G}, \mathbf{B}, \Phi)$ is called a *GDS* if and only if

$$(\mathbf{G}(\mathbf{x}, \dot{\mathbf{x}}) + \mathbf{\Xi}_{\mathbf{G}}(\mathbf{x}, \dot{\mathbf{x}})) \ddot{\mathbf{x}} + \mathbf{\xi}_{\mathbf{G}}(\mathbf{x}, \dot{\mathbf{x}}) = -\nabla_{\mathbf{x}} \Phi(\mathbf{x}) - \mathbf{B}(\mathbf{x}, \dot{\mathbf{x}}) \dot{\mathbf{x}}, \quad (3)$$

where $\mathbf{\Xi}_{\mathbf{G}}(\mathbf{x}, \dot{\mathbf{x}}) := \frac{1}{2} \sum_{i=1}^m \dot{x}_i \partial_{\dot{\mathbf{x}}} \mathbf{g}_i(\mathbf{x}, \dot{\mathbf{x}})$, $\mathbf{\xi}_{\mathbf{G}}(\mathbf{x}, \dot{\mathbf{x}}) := \dot{\mathbf{G}}(\mathbf{x}, \dot{\mathbf{x}}) \dot{\mathbf{x}} - \frac{1}{2} \nabla_{\mathbf{x}} (\dot{\mathbf{x}}^\top \mathbf{G}(\mathbf{x}, \dot{\mathbf{x}}) \dot{\mathbf{x}})$, and $\dot{\mathbf{G}}(\mathbf{x}, \dot{\mathbf{x}}) := [\partial_{\dot{\mathbf{x}}} \mathbf{g}_i(\mathbf{x}, \dot{\mathbf{x}}) \dot{\mathbf{x}}]_{i=1}^m$. We refer to $\mathbf{G}(\mathbf{x}, \dot{\mathbf{x}})$ as the *metric* matrix, $\mathbf{B}(\mathbf{x}, \dot{\mathbf{x}})$ as the *damping* matrix, and $\Phi(\mathbf{x})$ as the *potential* function which is lower-bounded. In addition, we define $\mathbf{M}(\mathbf{x}, \dot{\mathbf{x}}) := \mathbf{G}(\mathbf{x}, \dot{\mathbf{x}}) + \mathbf{\Xi}_{\mathbf{G}}(\mathbf{x}, \dot{\mathbf{x}})$ as the *inertia* matrix, which can be asymmetric. We say a GDS is *non-degenerate* if $\mathbf{M}(\mathbf{x}, \dot{\mathbf{x}})$ is nonsingular. We will assume (3) is non-degenerate so that it uniquely defines a differential equation and discuss the general case in Appendix A. $\mathbf{G}(\mathbf{x}, \dot{\mathbf{x}})$ induces

a metric of $\dot{\mathbf{x}}$, measuring its length as $\frac{1}{2}\dot{\mathbf{x}}^\top \mathbf{G}(\mathbf{x}, \dot{\mathbf{x}})\dot{\mathbf{x}}$. When $\mathbf{G}(\mathbf{x}, \dot{\mathbf{x}})$ depends on \mathbf{x} and $\dot{\mathbf{x}}$, it also induces the *curvature* terms $\Xi(\mathbf{x}, \dot{\mathbf{x}})$ and $\xi(\mathbf{x}, \dot{\mathbf{x}})$. In a particular case when $\mathbf{G}(\mathbf{x}, \dot{\mathbf{x}}) = \mathbf{G}(\mathbf{x})$, the GDSs reduce to the widely studied *simple mechanical systems* (SMSs) [15], $\mathbf{M}(\mathbf{x})\ddot{\mathbf{x}} + \mathbf{C}(\mathbf{x}, \dot{\mathbf{x}})\dot{\mathbf{x}} + \nabla_{\mathbf{x}}\Phi(\mathbf{x}) = -\mathbf{B}(\mathbf{x}, \dot{\mathbf{x}})\dot{\mathbf{x}}$; in this case $\mathbf{M}(\mathbf{x}) = \mathbf{G}(\mathbf{x})$ and the Coriolis force $\mathbf{C}(\mathbf{x}, \dot{\mathbf{x}})\dot{\mathbf{x}}$ is equal to $\xi_{\mathbf{G}}(\mathbf{x}, \dot{\mathbf{x}})$. The extension to velocity-dependent $\mathbf{G}(\mathbf{x}, \dot{\mathbf{x}})$ is important and non-trivial. As discussed in Section 3.6, it generalizes the dynamics of classical rigid-body systems, allowing the space to morph according to the velocity direction.

As its name suggests, GDSs possess geometric properties. Particularly, when $\mathbf{G}(\mathbf{x}, \dot{\mathbf{x}})$ is invertible, the left-hand side of (3) is related to a quantity $\mathbf{a}_{\mathbf{G}} = \ddot{\mathbf{x}} + \mathbf{G}(\mathbf{x}, \dot{\mathbf{x}})^{-1}(\Xi_{\mathbf{G}}(\mathbf{x}, \dot{\mathbf{x}})\ddot{\mathbf{x}} + \xi_{\mathbf{G}}(\mathbf{x}, \dot{\mathbf{x}}))$, known as the *geometric acceleration* (cf. Section 4.4). In short, we can think of (3) as setting $\mathbf{a}_{\mathbf{G}}$ along the negative natural gradient $-\mathbf{G}(\mathbf{x}, \dot{\mathbf{x}})^{-1}\nabla_{\mathbf{x}}\Phi(\mathbf{x})$ while imposing damping $-\mathbf{G}(\mathbf{x}, \dot{\mathbf{x}})^{-1}\mathbf{B}(\mathbf{x}, \dot{\mathbf{x}})\dot{\mathbf{x}}$.

4.2 Closure

Earlier, we mentioned that by tracking the geometry in `pullback` in (1), the task properties can be preserved. Here, we formalize the consistency of RMPflow as a closure of differential equations, named structured GDSs. Structured GDSs augment GDSs with information on how the metric matrix factorizes. Suppose \mathbf{G} has a structure \mathcal{S} that factorizes $\mathbf{G}(\mathbf{x}, \dot{\mathbf{x}}) = \mathbf{J}(\mathbf{x})^\top \mathbf{H}(\mathbf{y}, \dot{\mathbf{y}})\mathbf{J}(\mathbf{x})$, where $\mathbf{y} : \mathbf{x} \mapsto \mathbf{y}(\mathbf{x}) \in \mathbb{R}^n$ and $\mathbf{H} : \mathbb{R}^n \times \mathbb{R}^n \rightarrow \mathbb{R}_+^{n \times n}$, and $\mathbf{J}(\mathbf{x}) = \partial_{\mathbf{x}}\mathbf{y}$. We say the tuple $(\mathcal{M}, \mathbf{G}, \mathbf{B}, \Phi)_{\mathcal{S}}$ is a *structured GDS* if and only if

$$(\mathbf{G}(\mathbf{x}, \dot{\mathbf{x}}) + \Xi_{\mathbf{G}}(\mathbf{x}, \dot{\mathbf{x}}))\ddot{\mathbf{x}} + \eta_{\mathbf{G};\mathcal{S}}(\mathbf{x}, \dot{\mathbf{x}}) = -\nabla_{\mathbf{x}}\Phi(\mathbf{x}) - \mathbf{B}(\mathbf{x}, \dot{\mathbf{x}})\dot{\mathbf{x}} \quad (4)$$

where $\eta_{\mathbf{G};\mathcal{S}}(\mathbf{x}, \dot{\mathbf{x}}) := \mathbf{J}(\mathbf{x})^\top (\xi_{\mathbf{H}}(\mathbf{y}, \dot{\mathbf{y}}) + (\mathbf{H}(\mathbf{y}, \dot{\mathbf{y}}) + \Xi_{\mathbf{H}}(\mathbf{y}, \dot{\mathbf{y}}))\dot{\mathbf{J}}(\mathbf{x}, \dot{\mathbf{x}})\dot{\mathbf{x}})$. Note the metric and factorization *in combination* defines $\eta_{\mathbf{G};\mathcal{S}}$. As a special case, GDSs are structured GDSs with a *trivial* structure (i.e. $\mathbf{y} = \mathbf{x}$). Also, structured GDSs reduce to GDSs (i.e. the structure offers no extra information) if $\mathbf{G}(\mathbf{x}, \dot{\mathbf{x}}) = \mathbf{G}(\mathbf{x})$, or if $n, m = 1$ (cf. Appendix B.1). Given two structures, we say \mathcal{S}_a *preserves* \mathcal{S}_b if \mathcal{S}_a has the factorization (of \mathbf{H}) made by \mathcal{S}_b . In Section 4.4, we will show that structured GDSs are related to a geometric object, pullback connection, which turns out to be the coordinate-free version of `pullback`.

To show the closure property, we consider a parent node on \mathcal{M} with K child nodes on $\{\mathcal{N}_i\}_{i=1}^K$. We note that \mathbf{G}_i and \mathbf{B}_i can be functions of both \mathbf{y}_i and $\dot{\mathbf{y}}_i$.

Theorem 1. *Let the i th child node follow $(\mathcal{N}_i, \mathbf{G}_i, \mathbf{B}_i, \Phi_i)_{\mathcal{S}_i}$ and have coordinate \mathbf{y}_i . Let $\mathbf{f}_i = -\eta_{\mathbf{G}_i;\mathcal{S}_i} - \nabla_{\mathbf{y}_i}\Phi_i - \mathbf{B}_i\dot{\mathbf{y}}_i$ and $\mathbf{M}_i = \mathbf{G}_i + \Xi_{\mathbf{G}_i}$. If $[\mathbf{f}, \mathbf{M}]^{\mathcal{M}}$ of the parent node is given by `pullback` with $\{[\mathbf{f}_i, \mathbf{M}_i]^{\mathcal{N}_i}\}_{i=1}^K$ and \mathbf{M} is non-singular, the parent node follows $(\mathcal{M}, \mathbf{G}, \mathbf{B}, \Phi)_{\mathcal{S}}$, where $\mathbf{G} = \sum_{i=1}^K \mathbf{J}_i^\top \mathbf{G}_i \mathbf{J}_i$, $\mathbf{B} = \sum_{i=1}^K \mathbf{J}_i^\top \mathbf{B}_i \mathbf{J}_i$, $\Phi = \sum_{i=1}^K \Phi_i \circ \mathbf{y}_i$, \mathcal{S} preserves \mathcal{S}_i , and $\mathbf{J}_i = \partial_{\mathbf{x}}\mathbf{y}_i$. Particularly, if \mathbf{G}_i is velocity-free and the child nodes are GDSs, the parent node follows $(\mathcal{M}, \mathbf{G}, \mathbf{B}, \Phi)$.*

Theorem 1 shows structured GDSs are closed under `pullback`. It means that the differential equation of a structured GDS with a tree-structured task map can be computed by recursively applying `pullback` from the leaves to the root.

Corollary 1. *If all leaf nodes follow GDSs and \mathbf{M}_r at the root node is nonsingular, then the root node follows $(\mathcal{C}, \mathbf{G}, \mathbf{B}, \Phi)_{\mathcal{S}}$ as recursively defined by Theorem 1.*

4.3 Stability

By the closure property above, we analyze the stability of RMPflow when the leaf nodes are (structured) GDSs. For compactness, we will abuse the notation to write $\mathbf{M} = \mathbf{M}_r$. Suppose \mathbf{M} is nonsingular and let $(\mathcal{C}, \mathbf{G}, \mathbf{B}, \Phi)_S$ be the resultant structured GDS at the root node. We consider a Lyapunov candidate $V(\mathbf{q}, \dot{\mathbf{q}}) = \frac{1}{2}\dot{\mathbf{q}}^\top \mathbf{G}(\mathbf{q}, \dot{\mathbf{q}})\dot{\mathbf{q}} + \Phi(\mathbf{q})$ and derive its rate using properties of structured GDSs.

Proposition 1. *For $(\mathcal{C}, \mathbf{G}, \mathbf{B}, \Phi)_S$, $\dot{V}(\mathbf{q}, \dot{\mathbf{q}}) = -\dot{\mathbf{q}}^\top \mathbf{B}(\mathbf{q}, \dot{\mathbf{q}})\dot{\mathbf{q}}$.*

Proposition 1 directly implies the stability of structured GDSs by invoking LaSalle’s invariance principle [31]. Here we summarize the result without proof.

Corollary 2. *For $(\mathcal{C}, \mathbf{G}, \mathbf{B}, \Phi)_S$, if $\mathbf{G}(\mathbf{q}, \dot{\mathbf{q}}), \mathbf{B}(\mathbf{q}, \dot{\mathbf{q}}) \succ 0$, the system converges to a forward invariant set $\mathcal{C}_\infty := \{(\mathbf{q}, \dot{\mathbf{q}}) : \nabla_{\mathbf{q}}\Phi(\mathbf{q}) = 0, \dot{\mathbf{q}} = 0\}$.*

To show the stability of RMPflow, we need to further check when the assumptions in Corollary 2 hold. The condition $\mathbf{B}(\mathbf{q}, \dot{\mathbf{q}}) \succ 0$ is easy to satisfy: by Theorem 1, $\mathbf{B}(\mathbf{q}, \dot{\mathbf{q}}) \succeq 0$; to strictly ensure definiteness, we can copy \mathcal{C} into an additional child node with a (small) positive-definite damping matrix. The condition on $\mathbf{G}(\mathbf{q}, \dot{\mathbf{q}}) \succ 0$ can be satisfied similarly. In addition, we need to verify the assumption that \mathbf{M} is nonsingular. Here we provide a sufficient condition. When satisfied, it implies the global stability of RMPflow.

Theorem 2. *Suppose every leaf node is a GDS with a metric matrix in the form $\mathbf{R}(\mathbf{x}) + \mathbf{L}(\mathbf{x})^\top \mathbf{D}(\mathbf{x}, \dot{\mathbf{x}})\mathbf{L}(\mathbf{x})$ for differentiable functions \mathbf{R}, \mathbf{L} , and \mathbf{D} satisfying $\mathbf{R}(\mathbf{x}) \succeq 0$, $\mathbf{D}(\mathbf{x}, \dot{\mathbf{x}}) = \text{diag}((d_i(\mathbf{x}, \dot{y}_i))_{i=1}^n) \succeq 0$, and $\dot{y}_i \partial_{\dot{y}_i} d_i(\mathbf{x}, \dot{y}_i) \geq 0$, where \mathbf{x} is the coordinate of the leaf-node manifold and $\dot{\mathbf{y}} = \mathbf{L}\dot{\mathbf{x}} \in \mathbb{R}^n$. It holds $\Xi_{\mathbf{G}}(\mathbf{q}, \dot{\mathbf{q}}) \succeq 0$. If further $\mathbf{G}(\mathbf{q}, \dot{\mathbf{q}}), \mathbf{B}(\mathbf{q}, \dot{\mathbf{q}}) \succ 0$, then $\mathbf{M} \in \mathbb{R}_{++}^{d \times d}$, and the global RMP generated by RMPflow converges to the forward invariant set \mathcal{C}_∞ in Corollary 2.*

A particular condition in Theorem 2 is when all the leaf nodes with velocity dependent metric are 1D. Suppose $x \in \mathbb{R}$ is its coordinate and $g(x, \dot{x})$ is its metric matrix. The sufficient condition essentially boils down to $g(x, \dot{x}) \geq 0$ and $\dot{x} \partial_{\dot{x}} g(x, \dot{x}) \geq 0$. This means that, given any $x \in \mathbb{R}$, $g(x, 0) = 0$, $g(x, \dot{x})$ is non-decreasing when $\dot{x} > 0$, and non-increasing when $\dot{x} < 0$. This condition is satisfied by the collision avoidance policy in Section 3.6.

4.4 Invariance

We now discuss the coordinate-free geometric properties of $(\mathcal{C}, \mathbf{G}, \mathbf{B}, \Phi)_S$ generated by RMPflow. Due to space constraint, we only summarize the results (please see Appendix B.4 and, e.g., [32]). Here we assume that \mathbf{G} is positive-definite.

We first present the coordinate-free version of GDSs (i.e. the structure is trivial) by using a geometric object called *affine connection*, which defines how tangent spaces on a manifold are related. Let $T\mathcal{C}$ denote the tangent bundle of \mathcal{C} , which is a natural manifold to describe the state space. We first show that a GDS on \mathcal{C} can be written in terms of a unique, asymmetric affine connection ${}^G\nabla$ that is compatible with a Riemannian metric G (defined by \mathbf{G}) on $T\mathcal{C}$. It is important to note that G is defined on $T\mathcal{C}$ *not* the original manifold \mathcal{C} . As the metric matrix in a GDS can be velocity dependent, we need a larger manifold.

Theorem 3. *Let G be a Riemannian metric on TC such that, for $s = (q, v) \in TC$, $G(s) = G_{ij}^v(s)dq^i \otimes dq^j + G_{ij}^a dv^i \otimes dv^j$, where $G_{ij}^v(s)$ and G_{ij}^a are symmetric and positive-definite, and $G_{ij}^v(\cdot)$ is differentiable. Then there is a unique affine connection ${}^G\nabla$ that is compatible with G and satisfies, $\Gamma_{i,j}^k = \Gamma_{ji}^k$, $\Gamma_{i,j+d}^k = 0$, and $\Gamma_{i+d,j+d}^k = \Gamma_{j+d,i+d}^k$, for $i, j = 1, \dots, d$ and $k = 1, \dots, 2d$. In coordinates, if $G_{ij}^v(\dot{q})$ is identified as $\mathbf{G}(\mathbf{q}, \dot{\mathbf{q}})$, then $\text{pr}_3({}^G\nabla_{\dot{q}}\ddot{q})$ can be written as $\mathbf{a}_{\mathbf{G}} := \ddot{\mathbf{q}} + \mathbf{G}(\mathbf{q}, \dot{\mathbf{q}})^{-1}(\boldsymbol{\xi}_{\mathbf{G}}(\mathbf{q}, \dot{\mathbf{q}}) + \boldsymbol{\Xi}_{\mathbf{G}}(\mathbf{q}, \dot{\mathbf{q}})\dot{\mathbf{q}})$, where $\text{pr}_3 : (\mathbf{q}, \mathbf{v}, \mathbf{u}, \mathbf{a}) \mapsto \mathbf{u}$ is a projection.*

We call $\text{pr}_3({}^G\nabla_{\dot{q}}\ddot{q})$ the *geometric acceleration* of $q(t)$ with respect to ${}^G\nabla$. It is a coordinate-free object, because pr_3 is defined independent of the choice of chart of \mathcal{C} . By Theorem 3, it is clear that a GDS can be written abstractly as $\text{pr}_3({}^G\nabla_{\dot{q}}\ddot{q}) = (\text{pr}_3 \circ G^\sharp \circ F)(s)$, where $F : s \mapsto -d\Phi(s) - B(s)$ defines the covectors due to the potential function and damping, and $G^\sharp : T^*TC \rightarrow TTC$ denotes the inverse of G . In coordinates, it reads as $\ddot{\mathbf{q}} + \mathbf{G}(\mathbf{q}, \dot{\mathbf{q}})^{-1}(\boldsymbol{\xi}_{\mathbf{G}}(\mathbf{q}, \dot{\mathbf{q}}) + \boldsymbol{\Xi}_{\mathbf{G}}(\mathbf{q}, \dot{\mathbf{q}})\dot{\mathbf{q}}) = -\mathbf{G}(\mathbf{q}, \dot{\mathbf{q}})^{-1}(\nabla_{\mathbf{q}}\Phi(\mathbf{q}) + \mathbf{B}(\mathbf{q}, \dot{\mathbf{q}})\dot{\mathbf{q}})$, which is exactly (3).

Next we present a coordinate-free representation of RMPflow.

Theorem 4. *Suppose \mathcal{C} is related to K leaf-node task spaces by maps $\{\psi_i : \mathcal{C} \rightarrow \mathcal{T}_i\}_{i=1}^K$ and the i th task space \mathcal{T}_i has an affine connection ${}^{G_i}\nabla$ on $T\mathcal{T}_i$, as defined in Theorem 3, and a covector function F_i defined by some potential and damping as described above. Let ${}^G\bar{\nabla} = \sum_{i=1}^K T\psi_i^* {}^{G_i}\nabla$ be the pullback connection, $G = \sum_{i=1}^K T\psi_i^* G_i$ be the pullback metric, and $F = \sum_{i=1}^K T\psi_i^* F_i$ be the pullback covector, where $T\psi_i^* : T^*T\mathcal{T}_i \rightarrow T^*TC$. Then ${}^G\bar{\nabla}$ is compatible with G , and $\text{pr}_3({}^G\bar{\nabla}_{\dot{q}}\ddot{q}) = (\text{pr}_3 \circ G^\sharp \circ F)(s)$ can be written as $\ddot{\mathbf{q}} + \mathbf{G}(\mathbf{q}, \dot{\mathbf{q}})^{-1}(\boldsymbol{\eta}_{\mathbf{G},s}(\mathbf{q}, \dot{\mathbf{q}}) + \boldsymbol{\Xi}_{\mathbf{G}}(\mathbf{q}, \dot{\mathbf{q}})\dot{\mathbf{q}}) = -\mathbf{G}(\mathbf{q}, \dot{\mathbf{q}})^{-1}(\nabla_{\mathbf{q}}\Phi(\mathbf{q}) + \mathbf{B}(\mathbf{q}, \dot{\mathbf{q}})\dot{\mathbf{q}})$. In particular, if G is velocity-independent, then ${}^G\bar{\nabla} = {}^G\nabla$.*

Theorem 4 says that the structured GDS $(\mathcal{C}, \mathbf{G}, \mathbf{B}, \Phi)_{\mathcal{S}}$ can be written abstractly, without coordinates, using the pullback of task-space covectors, metrics, and asymmetric affine connections (that are defined in Theorem 3). In other words, the recursive calls of `pullback` in the backward pass of RMPflow is indeed performing “pullback” of geometric objects. Theorem 4 also shows, when G is velocity-independent, the pullback of connection and the pullback of metric commutes. In this case, ${}^G\bar{\nabla} = {}^G\nabla$, which is equivalent to the Levi-Civita connection of G . The loss of commutativity in general is due to the asymmetric definition of the connection in Theorem 3, which however is necessary to derive a control law of acceleration, without further referring to higher-order time derivatives.

4.5 Related Approaches

While here we focus on the special case of RMPflow with GDSs, this family already covers a wide range of reactive policies commonly used in practice. For example, when the task metric is Euclidean (i.e. constant), RMPflow recovers OSC (and its variants) [10, 19, 11, 12, 20]. When the task metric is only configuration dependent, RMPflow can be viewed as performing energy shaping to combine multiple SMSs in geometric control [15]. Further, RMPflow allows using velocity dependent metrics, generating behaviors all those previous rigid mechanics-based approaches fail to model. We also note that RMPflow can be

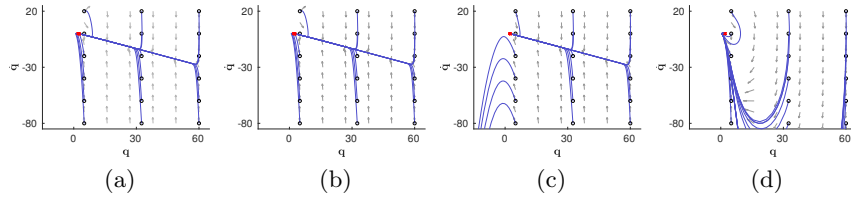


Fig. 2: Phase portraits (gray) and integral curves (blue; from black circles to red crosses) of 1D example. (a) Desired behavior. (b) With curvature terms. (c) Without curvature terms. (d) Without curvature terms but with nonlinear damping.

easily modified to incorporate exogenous time-varying inputs (e.g. forces to realize impedance control [18] or learned perturbations as in DMPs [29]). In computation, the structure of RMPflow in natural-formed RMPs resembles the classical Recursive Newton-Euler algorithm [17, 33] (see Appendix C). Alternatively, the canonical form of RMPflow in (2) resembles Gauss’ Principle [11, 12], but with a curvature correction $\Xi_{\mathbf{G}}$ on the inertia matrix (suggested by Theorem 1) to account for velocity dependent metrics. Thus, we can view RMPflow as a natural generalization of these approaches to a broader class of non-Euclidean behaviors.

5 Experiments

We perform controlled experiments to study the curvature effects of nonlinear metrics, which is important for stability and collision avoidance. We then perform several full-body experiments (video: <https://youtu.be/F14WvsXQDzo>) to demonstrate the capabilities of RMPflow on high-DOF manipulation problems in clutter, and implement an integrated vision-and-motion system on two physical robots.

5.1 Controlled Experiments

1D Example Let $\mathbf{q} \in \mathbb{R}$. We consider a barrier-type task map $\mathbf{x} = 1/\mathbf{q}$ and define a GDS in (3) with $\mathbf{G} = 1$, $\Phi(\mathbf{x}) = \frac{1}{2}(\mathbf{x} - \mathbf{x}_0)^2$, and $\mathbf{B} = (1 + 1/\mathbf{x})$, where $\mathbf{x}_0 > 0$. Using the GDS, we can define an RMP $[-\nabla_{\mathbf{x}}\Phi - \mathbf{B}\dot{\mathbf{x}} - \xi_{\mathbf{G}}, \mathbf{M}]^{\mathbb{R}}$, where \mathbf{M} and $\xi_{\mathbf{G}}$ are defined according to Section 4.1. We use this example to study the effects of $\dot{\mathbf{J}}\dot{\mathbf{q}}$ in pullback (1), where we define $\mathbf{J} = \partial_{\mathbf{q}}\mathbf{x}$. Fig. 2 compares the desired behavior (Fig. 2a) and the behaviors of correct/incorrect pullback. If pullback is performed correctly with $\dot{\mathbf{J}}\dot{\mathbf{q}}$, the behavior matches the designed one (Fig. 2b). By contrast, if $\dot{\mathbf{J}}\dot{\mathbf{q}}$ is ignored, the observed behavior becomes inconsistent and unstable (Fig. 2c). While the instability of neglecting $\dot{\mathbf{J}}\dot{\mathbf{q}}$ can be recovered with a damping $\mathbf{B} = (1 + \frac{\dot{\mathbf{x}}^2}{\mathbf{x}})$ nonlinear in $\dot{\mathbf{x}}$ (suggested in [20]), the behavior remains inconsistent (Fig. 2d).

2D Example We consider a 2D goal-reaching task with collision avoidance and study the effects of velocity dependent metrics. First, we define an RMP (a GDS as in Section 3.6) in $\mathbf{x} = d(\mathbf{q})$ (the 1D task space of the distance to the obstacle). We pick a metric $\mathbf{G}(\mathbf{x}, \dot{\mathbf{x}}) = w(\mathbf{x})u(\dot{\mathbf{x}})$, where $w(\mathbf{x}) = 1/\mathbf{x}^4$ increases if the particle is *close* to the obstacle and $u(\dot{\mathbf{x}}) = \epsilon + \min(0, \dot{\mathbf{x}})\dot{\mathbf{x}}$ (where $\epsilon \geq 0$), increases if it moves *towards* the obstacle. As this metric is non-constant, the GDS has curvature terms $\Xi_{\mathbf{G}} = \frac{1}{2}\dot{\mathbf{x}}w(\mathbf{x})\partial_{\dot{\mathbf{x}}}u(\dot{\mathbf{x}})$ and $\xi_{\mathbf{G}} = \frac{1}{2}\dot{\mathbf{x}}^2u(\dot{\mathbf{x}})\partial_{\mathbf{x}}w(\mathbf{x})$. These

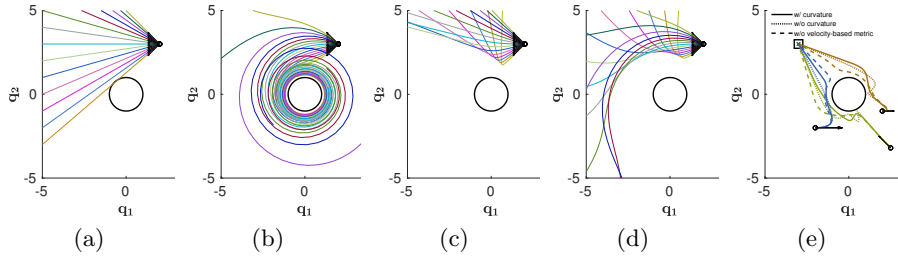


Fig. 3: 2D example; initial positions (small circle) and velocities (arrows). (a-d) Obstacle (circle) avoidance: (a) w/o curvature terms and w/o potential. (b) w/ curvature terms and w/o potential. (c) w/o curvature terms and w/ potential. (d) w/ curvature terms and w/ potential. (e) Combined obstacle avoidance and goal (square) reaching.

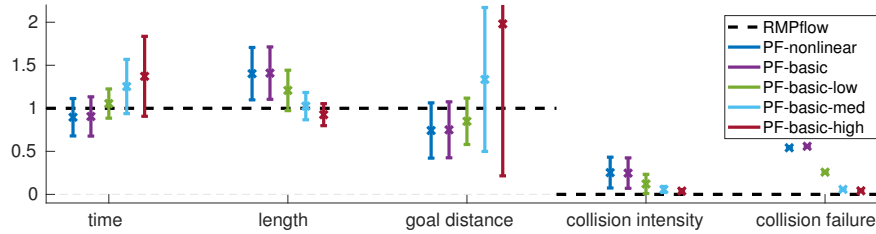


Fig. 4: Results for reaching experiments. Though some methods achieve a shorter goal distance than RMPflow in successful trials, they end up in collision in most the trials.

curvature terms along with $\mathbf{J}\dot{\mathbf{q}}$ produce an acceleration that lead to natural obstacle avoidance behavior, coaxing the system toward isocontours of the obstacle (Fig. 3b). On the other hand, when the curvature terms are ignored, the particle travels in straight lines with constant velocity (Fig. 3a). To define the full collision avoidance RMP, we introduce a barrier-type potential $\Phi(\mathbf{x}) = \frac{1}{2}\alpha w(\mathbf{x})^2$ to create extra repulsive forces, where $\alpha \geq 0$. A comparison of the curvature effects in this setting is shown in Fig. 3c and 3d (with $\alpha = 1$). Next, we use RMPflow to combine the collision avoidance RMP above (with $\alpha = 0.001$) and an attractor RMP. Let \mathbf{q}_g be the goal. The attractor RMP is a GDS in the task space $\mathbf{y} = \mathbf{q} - \mathbf{q}_g$ with a metric $w(\mathbf{y})\mathbf{I}$, a damping $\eta w(\mathbf{y})\mathbf{I}$, and a potential that is zero at $\mathbf{y} = 0$, where $\eta > 0$ (see Appendix D.4). Fig. 3e shows the trajectories of the combined RMP. The combined non-constant metrics generate a behavior that transitions smoothly towards the goal while heading away from the obstacle. When the curvature terms are ignored (for both RMPs), the trajectories oscillate near the obstacle. In practice, this can result in jittery behavior on manipulators. When the metric is not velocity-based ($\mathbf{G}(\mathbf{x}) = w(\mathbf{x})$) the behavior is less efficient in breaking free from the obstacle to go toward the goal.

5.2 System Experiments

Reaching-through-clutter Experiments We compare RMPflow with OSC, (i.e. potential fields (PF) with dynamics reshaping), denoted as PF-basic, and a variant, denoted PF-nonlinear, which scales the collision-avoidance weights nonlinearly as a function of obstacle proximity. We highlight the results here; Appendix E provides additional details, and the supplementary video shows footage of the trials. In both baselines, the collision-avoidance task spaces are

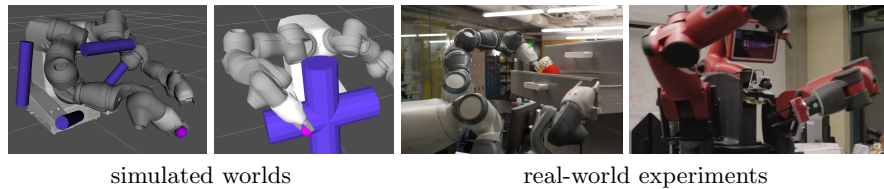


Fig. 5: Two of the six simulated worlds in the reaching experiments (left), and the two physical dual-arm platforms in the full system experiment (right).

specified by control points along the robot’s body (rather than the distance space used in RMPflow) with an isotropic metric $\mathbf{G} = w(\mathbf{x})\mathbf{I}$ (here $w(\mathbf{x}) = w_o \in \mathbb{R}_+$ for PF-basic and $w(\mathbf{x}) \in [0, w_o]$ for PF-nonlinear, where w_o is the max metric size used in RMPflow). The task-space policies of both variants follow GDSs, but without the curvature terms (see Appendix E).

Fig. 4 summarizes their performance. We measure time-to-goal, C-space path length (assessing economy of motion), achievable distance-to-goal (efficacy in solving the problem), collision intensity (percent time in collision *given* a collision), collision failures (percent trials with collisions). The isotropic metrics, across multiple settings, fail to match the speed and precision achieved by RMPflow. Higher-weight settings tend to have fewer collisions and better economy of motion, but at the expense of efficiency. Additionally, adding non-linear weights as in PF-nonlinear does not seem to help. The decisive factor of RMPflow’s performance is rather its non-isotropic metric, which encodes directional importance around obstacles in combing policies.

System Integration for Real-Time Reactive Motion Generation We present an integrated system for vision-driven dual arm manipulation on two robotic platforms, the ABB YuMi robot and the Rethink Baxter robot (Fig. 5) (see the supplementary video). Our system uses the real-time optimization-based tracking algorithm DART [34] to communicate with the RMP system, receiving prior information on robot configuration and sending tracking updates of world state. The system is tested in multiple real-world manipulation problems, like picking up trash in clutter, reactive manipulation of a cabinet with human perturbation, active lead-through (compliant guiding of the arms with world-aware collision controllers) and pick-and-place of objects into a drawer which the robot opens and closes. Please see Appendix F for the details of the experiments.

6 Conclusion

We propose an efficient policy synthesis framework, RMPflow, for generating policies with non-Euclidean behavior, including motion with velocity dependent metrics that are new to the literature. In design, RMPflow is implemented as a computational graph, which can geometrically consistently combine subtask policies into a global policy for the robot. In theory, we provide conditions for stability and show that RMPflow is intrinsically coordinate-free. In the experiments, we demonstrate that RMPflow can generate smooth and natural motion for various tasks, when proper subtask RMPs are specified. Future work is to

further relax the requirement on the quality of designing subtask RMPs by introducing learning components into RMPflow for additional flexibility.

References

1. Rimon, E., Koditschek, D.: The construction of analytic diffeomorphisms for exact robot navigation on star worlds. *Transactions of the American Mathematical Society* 327(1), 71–116 (1991)
2. Ratliff, N., Toussaint, M., Schaal, S.: Understanding the geometry of workspace obstacles in motion optimization. In: *IEEE International Conference on Robotics and Automation (ICRA)* (2015)
3. Ivan, V., Zarubin, D., Toussaint, M., Komura, T., Vijayakumar, S.: Topology-based representations for motion planning and generalization in dynamic environments with interactions. *International Journal of Robotics Research (IJRR)* 32(9-10), 1151–1163 (2013)
4. Watterson, M., Liu, S., Sun, K., Smith, T., Kumar, V.: Trajectory optimization on manifolds with applications to $SO(3)$ and R3XS2. In: *Robotics: Science and Systems (RSS)* (2018)
5. Toussaint, M.: Robot trajectory optimization using approximate inference. In: *ICML*. pp. 1049–1056 (2009)
6. LaValle, S.M.: *Planning Algorithms*. Cambridge University Press, Cambridge, U.K. (2006), available at <http://planning.cs.uiuc.edu/>
7. Karaman, S., Frazzoli, E.: Sampling-based algorithms for optimal motion planning. *International Journal of Robotics Research (IJRR)* 30(7), 846–894 (2011), <http://arxiv.org/abs/1105.1186>
8. Gammell, J.D., Srinivasa, S.S., Barfoot, T.D.: Batch Informed Trees (BIT*): Sampling-based optimal planning via the heuristically guided search of implicit random geometric graphs. In: *IEEE International Conference on Robotics and Automation (ICRA)* (2015)
9. Mukadam, M., Dong, J., Yan, X., Dellaert, F., Boots, B.: Continuous-time Gaussian process motion planning via probabilistic inference. *arXiv preprint arXiv:1707.07383* (2017)
10. Khatib, O.: A unified approach for motion and force control of robot manipulators: The operational space formulation. *IEEE Journal on Robotics and Automation* 3(1), 43–53 (1987)
11. Peters, J., Mistry, M., Udwadia, F.E., Nakanishi, J., Schaal, S.: A unifying framework for robot control with redundant DOFs. *Autonomous Robots* 1, 1–12 (2008)
12. Udwadia, F.E.: A new perspective on the tracking control of nonlinear structural and mechanical systems. *Proceedings of the Royal Society of London A: Mathematical, Physical and Engineering Sciences* 459(2035), 1783–1800 (2003), <http://rspa.royalsocietypublishing.org/content/459/2035/1783>
13. Kappler, D., Meier, F., Issac, J., Mainprice, J., Garcia Cifuentes, C., Wüthrich, M., Berenz, V., Schaal, S., Ratliff, N., Bohg, J.: Real-time perception meets reactive motion generation. *IEEE Robotics and Automation Letters* 3(3), 1864–1871 (2018), <https://arxiv.org/abs/1703.03512>
14. Mukadam, M., Cheng, C.A., Yan, X., Boots, B.: Approximately optimal continuous-time motion planning and control via probabilistic inference. In: *IEEE International Conference on Robotics and Automation (ICRA)* (2017)
15. Bullo, F., Lewis, A.D.: *Geometric control of mechanical systems: modeling, analysis, and design for simple mechanical control systems*, vol. 49. Springer Science & Business Media (2004)

16. Ratliff, N.D., Issac, J., Kappler, D., Birchfield, S., Fox, D.: Riemannian motion policies. arXiv preprint arXiv:1801.02854 (2018)
17. Walker, M.W., Orin, D.E.: Efficient dynamic computer simulation of robotic mechanisms. *Journal of Dynamic Systems, Measurement, and Control* 104(3), 205–211 (1982)
18. Albu-Schaffer, A., Hirzinger, G.: Cartesian impedance control techniques for torque controlled light-weight robots. In: *IEEE International Conference on Robotics and Automation (ICRA)*. vol. 1, pp. 657–663 (2002)
19. Sentis, L., Khatib, O.: A whole-body control framework for humanoids operating in human environments. In: *IEEE International Conference on Robotics and Automation (ICRA)*. pp. 2641–2648 (2006)
20. Lo, S.Y., Cheng, C.A., Huang, H.P.: Virtual impedance control for safe human-robot interaction. *Journal of Intelligent & Robotic Systems* 82(1), 3–19 (2016)
21. Erez, T., Lowrey, K., Tassa, Y., Kumar, V., Kolev, S., Todorov, E.: An integrated system for real-time model-predictive control of humanoid robots. In: *IEEE/RAS International Conference on Humanoid Robots* (2013)
22. Todorov, E.: Optimal control theory. In *Bayesian Brain: Probabilistic Approaches to Neural Coding* pp. 269–298 (2006)
23. Liegeois, A.: Automatic supervisory control of the configuration and behaviour of multibody mechanisms. *IEEE Transactions on Systems, Man and Cybernetics* 7(12), 868–871 (1977)
24. Ratliff, N., Zucker, M., Bagnell, J.A.D., Srinivasa, S.: CHOMP: Gradient optimization techniques for efficient motion planning. In: *IEEE International Conference on Robotics and Automation (ICRA)* (2009)
25. Mukadam, M., Yan, X., Boots, B.: Gaussian process motion planning. In: *IEEE Conference on Robotics and Automation (ICRA)* (2016)
26. Dong, J., Mukadam, M., Dellaert, F., Boots, B.: Motion planning as probabilistic inference using Gaussian processes and factor graphs. In: *Robotics: Science and Systems (RSS)* (2016)
27. Nakanishi, J., Cory, R., Mistry, M., Peters, J., Schaal, S.: Operational space control: A theoretical and empirical comparison. *International Journal of Robotics Research (IJRR)* 6, 737–757 (2008)
28. Platt, R., Abdallah, M.E., Wampler, C.W.: Multiple-priority impedance control. In: *IEEE International Conference on Robotics and Automation (ICRA)*. pp. 6033–6038. Citeseer (2011)
29. Ijspeert, A.J., Nakanishi, J., Hoffmann, H., Pastor, P., Schaal, S.: Dynamical movement primitives: Learning attractor models for motor behaviors. *Neural Computation* 25(2), 328–373 (Feb 2013)
30. Lewis, A.D.: The geometry of the maximum principle for affine connection control systems (2000)
31. Khalil, H.K.: *Nonlinear systems*. Prentice-Hall, New Jersey 2(5), 5–1 (1996)
32. Lee, J.M., Chow, B., Chu, S.C., Glickenstein, D., Guenther, C., Isenberg, J., Ivey, T., Knopf, D., Lu, P., Luo, F., et al.: *Manifolds and differential geometry*. *Topology* 643, 658 (2009)
33. Featherstone, R.: *Rigid Body Dynamics Algorithms*. Springer (2008)
34. Schmidt, T., Newcombe, R., Fox, D.: DART: Dense articulated real-time tracking with consumer depth cameras. *Autonomous Robots* 39(3) (2015)
35. Taylor, J.R.: *Classical Mechanics*. University Science Books (2005)
36. Udwadia, F.E., Kalaba, R.E.: *Analytical Dynamics: A New Approach*. Cambridge University Press (1996)

Appendices

A Geometric Dynamical Systems

Here we summarize details and properties of GDSs introduced in Section 4.1.

A.1 From Geometric Mechanics to GDSs

Our study of GDSs is motivated by geometric mechanics. Many formulations of mechanics exist, including Lagrangian mechanics [35] and the aforementioned Gauss’s Principle of Least Constraint [36]—They are all equivalent, implicitly sharing the same mathematical structure. In that sense, geometric mechanics, which models physical systems as geodesic flow on Riemannian manifolds, is the most explicit of these, revealing directly the underlying manifold structure and connecting to the broad mathematical tool set from Riemannian geometry. These connections enable us here to generalize beyond the previous simple mechanical systems studied in [15] to non-classical systems that more naturally describe robotic behaviors with non-Euclidean geometric properties.

A.2 Degenerate GDSs

Let us recall the definition of GDSs.

Definition 1. Let $\mathbf{B} : \mathbb{R}^m \times \mathbb{R}^m \rightarrow \mathbb{R}_+^{m \times m}$ and let $\mathbf{G} : \mathbb{R}^m \times \mathbb{R}^m \rightarrow \mathbb{R}_+^{m \times m}$ and $\Phi : \mathbb{R}^m \rightarrow \mathbb{R}$ be differentiable. We say the tuple $(\mathcal{M}, \mathbf{G}, \mathbf{B}, \Phi)$ is a GDS if

$$\mathbf{M}(\mathbf{x}, \dot{\mathbf{x}})\ddot{\mathbf{x}} + \boldsymbol{\xi}_{\mathbf{G}}(\mathbf{x}, \dot{\mathbf{x}}) = -\nabla_{\mathbf{x}}\Phi(\mathbf{x}) - \mathbf{B}(\mathbf{x}, \dot{\mathbf{x}})\dot{\mathbf{x}} \quad (5)$$

where $\mathbf{M}(\mathbf{x}, \dot{\mathbf{x}}) = \mathbf{G}(\mathbf{x}, \dot{\mathbf{x}}) + \boldsymbol{\Xi}_{\mathbf{G}}(\mathbf{x}, \dot{\mathbf{x}})$.

For degenerate cases, $\mathbf{M}(\mathbf{x}, \dot{\mathbf{x}})$ can be singular and (5) define rather a family of differential equations. Degenerate cases are not uncommon; for example, the leaf-node dynamics could have \mathbf{G} being only positive semidefinite. Having degenerate GDSs does not change the properties that we have proved, but one must be careful about whether differential equation satisfying (5) exist. For example, the existence is handled by the assumption on \mathbf{M} in Theorem 1 and the assumption on \mathbf{M}_r in Corollary 1. For RMPflow, we only need that \mathbf{M}_r at the root node is non-singular. In other words, the natural-form RMP created by `pullback` at the root node can be resolved in the canonical-form RMP for policy execution. A sufficient and yet practical condition is provided in Theorem 2.

A.3 Geodesic and Stability

For GDSs, they possess a natural conservation property of kinematic energy, i.e. it travels along a geodesic defined by $\mathbf{G}(\mathbf{x}, \dot{\mathbf{x}})$ when there is no external perturbations due to Φ and \mathbf{B} . Note $\mathbf{G}(\mathbf{x}, \dot{\mathbf{x}})$ by definition may only be positive-semidefinite even when the system is non-degenerate; here we allow the geodesic

to be defined for a degenerate metric, meaning a curve whose instant length measured by the (degenerate) metric is constant.

This geometric feature is an important tool to establish the stability of non-degenerate GDSs; We highlight this nice geometric property below, which is a corollary of Proposition 1.

Corollary 3. *All non-degenerate GDSs in the form $(\mathcal{M}, \mathbf{G}, 0, 0)$ travel on geodesics. That is, $\dot{K}(\mathbf{x}, \dot{\mathbf{x}}) = 0$, where $K(\mathbf{x}, \dot{\mathbf{x}}) = \frac{1}{2} \dot{\mathbf{x}}^\top \mathbf{G}(\mathbf{x}, \dot{\mathbf{x}}) \dot{\mathbf{x}}$.*

Note that this property also hold for degenerate GDSs provided that differential equations satisfying (5) exist.

A.4 Curvature Term and Coriolis Force

The curvature term $\xi_{\mathbf{G}}$ in GDSs is highly related to the Coriolis force in the mechanics literature. This is not surprising, as from the analysis in Section 4.4 we know that $\xi_{\mathbf{G}}$ comes from the Christoffel symbols of the asymmetric connection. Recall it is defined as

$$\xi_{\mathbf{G}}(\mathbf{x}, \dot{\mathbf{x}}) := \ddot{\mathbf{G}}(\mathbf{x}, \dot{\mathbf{x}}) \dot{\mathbf{x}} - \frac{1}{2} \nabla_{\mathbf{x}} (\dot{\mathbf{x}}^\top \mathbf{G}(\mathbf{x}, \dot{\mathbf{x}}) \dot{\mathbf{x}})$$

We show their relationship explicitly below.

Lemma 1. *Let $\Gamma_{ijk} = \frac{1}{2}(\partial_{x_k} G_{ij} + \partial_{x_j} G_{ik} - \partial_{x_j} G_{jk})$ be the Christoffel symbol of the first kind with respect to $\mathbf{G}(\mathbf{x}, \dot{\mathbf{x}})$, where the subscript ij denotes the (i, j) element. Let $C_{ij} = \sum_{k=1}^d \dot{x}_k \Gamma_{ijk}$ and define $\mathbf{C}(\mathbf{x}, \dot{\mathbf{x}}) = (C_{ij})_{i,j=1}^m$. Then $\xi_{\mathbf{G}}(\mathbf{x}, \dot{\mathbf{x}}) = \mathbf{C}(\mathbf{x}, \dot{\mathbf{x}}) \dot{\mathbf{x}}$.*

Proof of Lemma 1. Suppose $\xi_{\mathbf{G}} = (\xi_i)_{i=1}^m$. We can compare the two definitions and verify they are indeed equivalent:

$$\begin{aligned} \xi_i &= \sum_{j,k=1}^d \dot{x}_j \dot{x}_k \partial_{x_j} G_{ik} - \frac{1}{2} \sum_{j,k=1}^d \dot{x}_j \dot{x}_k \partial_{x_i} G_{jk} \\ &= \frac{1}{2} \sum_{j,k=1}^d \dot{x}_j \dot{x}_k \partial_{x_k} G_{ij} + \frac{1}{2} \sum_{j,k=1}^d \dot{x}_j \dot{x}_k \partial_{x_j} G_{ik} - \frac{1}{2} \sum_{j,k=1}^d \dot{x}_j \dot{x}_k \partial_{x_i} G_{jk} \\ &= (\mathbf{C}(\mathbf{x}, \dot{\mathbf{x}}) \dot{\mathbf{x}})_i \end{aligned} \quad \blacksquare$$

B Proofs of RMPflow Analysis

B.1 Proof of Theorem 1

Theorem 1. *Let the i th child node follow $(\mathcal{N}_i, \mathbf{G}_i, \mathbf{B}_i, \Phi_i)_{\mathcal{S}_i}$ and have coordinate \mathbf{y}_i . Let $\mathbf{f}_i = -\boldsymbol{\eta}_{\mathbf{G}_i; \mathcal{S}_i} - \nabla_{\mathbf{y}_i} \Phi_i - \mathbf{B}_i \dot{\mathbf{y}}_i$ and $\mathbf{M}_i = \mathbf{G}_i + \boldsymbol{\Xi}_{\mathbf{G}_i}$. If $[\mathbf{f}, \mathbf{M}]^{\mathcal{M}}$ of the parent node is given by pullback with $\{[\mathbf{f}_i, \mathbf{M}_i]^{\mathcal{N}_i}\}_{i=1}^K$ and \mathbf{M} is non-singular, the parent node follows $(\mathcal{M}, \mathbf{G}, \mathbf{B}, \Phi)_{\mathcal{S}}$, where $\mathbf{G} = \sum_{i=1}^K \mathbf{J}_i^\top \mathbf{G}_i \mathbf{J}_i$, $\mathbf{B} = \sum_{i=1}^K \mathbf{J}_i^\top \mathbf{B}_i \mathbf{J}_i$, $\Phi = \sum_{i=1}^K \Phi_i \circ \mathbf{y}_i$, \mathcal{S} preserves \mathcal{S}_i , and $\mathbf{J}_i = \partial_{\mathbf{x}} \mathbf{y}_i$. Particularly, if \mathbf{G}_i is velocity-free and the child nodes are GDSs, the parent node follows $(\mathcal{M}, \mathbf{G}, \mathbf{B}, \Phi)$.*

Proof of Theorem 1. We will use the non-degeneracy assumption that $\mathbf{G} + \mathbf{\Xi}_{\mathbf{G}}$ (i.e. \mathbf{M} as we will show) is non-singular, so that the differential equation specified by an RMP in normal form or a (structured) GDS is unique. This assumption is made to simplify writing. At the end of the proof, we will show that this assumption only needs to be true at the root node of RMPflow.

The general case We first show the differential equation given by `pullback` is equivalent to the differential equation of pullback structured GDS $(\mathcal{M}, \mathbf{G}, \mathbf{B}, \Phi)_{\mathcal{S}}$. Under the non-degeneracy assumption, suppose \mathcal{S}_i factorizes \mathbf{G}_i as $\mathbf{G}_i = \mathbf{L}_i^{\top} \mathbf{H}_i \mathbf{L}_i$, where \mathbf{L}_i is some Jacobian matrix. On one hand, for `pullback`, because in the child node $\dot{\mathbf{y}}_i$ satisfies $(\mathbf{G}_i + \mathbf{\Xi}_{\mathbf{G}_i})\ddot{\mathbf{y}}_i = -\boldsymbol{\eta}_{\mathbf{G}_i; \mathcal{S}_i} - \nabla_{\mathbf{y}_i} \Phi_i - \mathbf{B}_i \dot{\mathbf{y}}_i$ (where by definition $\boldsymbol{\eta}_{\mathbf{G}_i; \mathcal{S}_i} = \mathbf{L}_i^{\top} (\boldsymbol{\xi}_{\mathbf{H}_i} + (\mathbf{H}_i + \mathbf{\Xi}_{\mathbf{H}_i}) \dot{\mathbf{L}}_i \dot{\mathbf{y}}_i)$), the `pullback` operator combines the child nodes into the differential equation at the parent node,

$$\mathbf{M} \ddot{\mathbf{x}} = \sum_{i=1}^K \mathbf{J}_i^{\top} \mathbf{M}_i (\ddot{\mathbf{y}}_i - \dot{\mathbf{J}}_i \dot{\mathbf{x}}) \quad (6)$$

where we recall $\mathbf{M} = \sum_{i=1}^K \mathbf{J}_i^{\top} \mathbf{M}_i \mathbf{J}_i$ is given by `pullback`. On the other hand, for $(\mathcal{M}, \mathbf{G}, \mathbf{B}, \Phi)_{\mathcal{S}}$ with \mathcal{S} preserving \mathcal{S}_i , its dynamics satisfy

$$(\mathbf{G} + \mathbf{\Xi}_{\mathbf{G}}) \ddot{\mathbf{x}} + \boldsymbol{\eta}_{\mathbf{G}; \mathcal{S}} = -\nabla_{\mathbf{x}} \Phi - \mathbf{B} \dot{\mathbf{x}} \quad (7)$$

where \mathbf{G} is factorized by \mathcal{S} into

$$\mathbf{G} = \begin{bmatrix} \mathbf{J}_1 \\ \vdots \\ \mathbf{J}_K \end{bmatrix}^{\top} \begin{bmatrix} \mathbf{G}_1 & & \\ & \ddots & \\ & & \mathbf{G}_K \end{bmatrix} \begin{bmatrix} \mathbf{J}_1 \\ \vdots \\ \mathbf{J}_K \end{bmatrix} = \begin{bmatrix} \mathbf{L}_1 \mathbf{J}_1 \\ \vdots \\ \mathbf{L}_K \mathbf{J}_K \end{bmatrix}^{\top} \begin{bmatrix} \mathbf{H}_1 & & \\ & \ddots & \\ & & \mathbf{H}_K \end{bmatrix} \begin{bmatrix} \mathbf{L}_1 \mathbf{J}_1 \\ \vdots \\ \mathbf{L}_K \mathbf{J}_K \end{bmatrix} =: \bar{\mathbf{J}}^{\top} \bar{\mathbf{H}} \bar{\mathbf{J}}$$

and the curvature term $\boldsymbol{\eta}_{\mathbf{G}; \mathcal{S}}$ by \mathcal{S} is given as $\boldsymbol{\eta}_{\mathbf{G}; \mathcal{S}} := \bar{\mathbf{J}}^{\top} (\boldsymbol{\xi}_{\bar{\mathbf{H}}} + (\bar{\mathbf{H}} + \mathbf{\Xi}_{\bar{\mathbf{H}}}) \dot{\bar{\mathbf{J}}} \dot{\mathbf{x}})$.

To prove the general statement, we will show (6) and (7) are equivalent. First, we introduce a lemma to write $\mathbf{\Xi}_{\mathbf{G}}$ in terms of $\mathbf{\Xi}_{\mathbf{G}_i}$ (proved later in this section).

Lemma 2. *Let \mathcal{M} and \mathcal{N} be two manifolds and let \mathbf{x} and $\mathbf{y}(\mathbf{x})$ be the coordinates. Define $\mathbf{M}(\mathbf{x}, \dot{\mathbf{x}}) = \mathbf{J}(\mathbf{x})^{\top} \mathbf{N}(\mathbf{y}, \dot{\mathbf{y}}) \mathbf{J}(\mathbf{x})$, where $\mathbf{J}(\mathbf{x}) = \partial_{\mathbf{x}} \mathbf{y}(\mathbf{x})$. Then*

$$\mathbf{\Xi}_{\mathbf{M}}(\mathbf{x}, \dot{\mathbf{x}}) = \mathbf{J}^{\top}(\mathbf{x}) \mathbf{\Xi}_{\mathbf{N}}(\mathbf{y}, \dot{\mathbf{y}}) \mathbf{J}(\mathbf{x})$$

Therefore, we see that on the LHSs

$$(\mathbf{G} + \mathbf{\Xi}_{\mathbf{G}}) \ddot{\mathbf{x}} = \mathbf{M} \ddot{\mathbf{x}}$$

and on the RHSs

$$\begin{aligned}
& \left(\sum_{i=1}^K \mathbf{J}_i^\top \mathbf{M}_i (\ddot{\mathbf{y}}_i - \dot{\mathbf{J}}_i \dot{\mathbf{x}}) \right) \\
&= \left(\sum_{i=1}^K \mathbf{J}_i^\top (-\boldsymbol{\eta}_{\mathbf{G}_i; \mathcal{S}_i} - \nabla_{\mathbf{y}_i} \Phi_i - \mathbf{B}_i \dot{\mathbf{y}}_i - (\mathbf{G}_i + \boldsymbol{\Xi}_{\mathbf{G}_i}) \dot{\mathbf{J}}_i \dot{\mathbf{x}}) \right) \\
&= \left(\sum_{i=1}^K \mathbf{J}_i^\top (-\mathbf{L}_i^\top (\boldsymbol{\xi}_{\mathbf{H}_i} + (\mathbf{H}_i + \boldsymbol{\Xi}_{\mathbf{H}_i}) \dot{\mathbf{L}}_i \dot{\mathbf{y}}_i) - (\mathbf{G}_i + \boldsymbol{\Xi}_{\mathbf{G}_i}) \dot{\mathbf{J}}_i \dot{\mathbf{x}}) \right) + \left(\sum_{i=1}^K \mathbf{J}_i^\top (-\nabla_{\mathbf{y}_i} \Phi_i - \mathbf{B}_i \dot{\mathbf{y}}_i) \right) \\
&= \left(\sum_{i=1}^K -\bar{\mathbf{J}}_i^\top \boldsymbol{\xi}_{\mathbf{H}_i} - \bar{\mathbf{J}}_i^\top (\mathbf{H}_i + \boldsymbol{\Xi}_{\mathbf{H}_i}) (\dot{\mathbf{L}}_i \mathbf{J}_i + \mathbf{L}_i \dot{\mathbf{J}}_i) \dot{\mathbf{x}} \right) - \nabla_{\mathbf{x}} \Phi - \mathbf{B} \dot{\mathbf{x}} \\
&= -\boldsymbol{\eta}_{\mathbf{G}; \mathcal{S}} - \nabla_{\mathbf{x}} \Phi - \mathbf{B} \dot{\mathbf{x}}
\end{aligned}$$

where the first equality is due to Lemma 2, the second equality is due to (6), and the third equality is due to the definition of structured GDSs. The above derivations show the equivalence between the RHSs and LHSs of (6) and (7), respectively. Therefore, when the non-degenerate assumption holds, (6) and (7) are equivalent.

The special case With the closure of structured GDSs proved, we next show the closure of GDSs under `pullback`, when the metric is only configuration-dependent. That is, we want to show that, when the metric is only configuration-dependent, the choice of structure does not matter. This amounts to show that $\boldsymbol{\xi}_{\mathbf{G}} = \boldsymbol{\eta}_{\mathbf{G}; \mathcal{S}}$ because by definition $\boldsymbol{\Xi}_i = 0$ and $\boldsymbol{\Xi} = 0$. Below we show how $\boldsymbol{\xi}_{\mathbf{G}}$ is written in terms of $\boldsymbol{\xi}_{\mathbf{G}_i}$ and $\boldsymbol{\Xi}_{\mathbf{G}_i}$ for general metric matrices and specialize it to the configuration-dependent special case (proved later in this section).

Lemma 3. *Let \mathcal{M} and \mathcal{N} be two manifolds and \mathbf{x} and $\mathbf{y}(\mathbf{x})$ be the coordinates. Suppose $\mathbf{M}(\mathbf{x}, \dot{\mathbf{x}})$ is structured as $\mathbf{J}(\mathbf{x})^\top \mathbf{N}(\mathbf{y}, \dot{\mathbf{y}}) \mathbf{J}(\mathbf{x})$, where $\mathbf{J}(\mathbf{x}) = \partial_{\mathbf{x}} \mathbf{y}(\mathbf{x})$. Then*

$$\begin{aligned}
\boldsymbol{\xi}_{\mathbf{M}}(\mathbf{x}, \dot{\mathbf{x}}) &= \mathbf{J}(\mathbf{x})^\top \left(\boldsymbol{\xi}_{\mathbf{N}}(\mathbf{y}, \dot{\mathbf{y}}) + (\mathbf{N}(\mathbf{y}, \dot{\mathbf{y}}) + 2\boldsymbol{\Xi}_{\mathbf{N}}(\mathbf{y}, \dot{\mathbf{y}})) \dot{\mathbf{J}}(\mathbf{x}, \dot{\mathbf{x}}) \dot{\mathbf{x}} \right) \\
&\quad - \dot{\mathbf{J}}(\mathbf{x}, \dot{\mathbf{x}})^\top \boldsymbol{\Xi}_{\mathbf{N}}(\mathbf{y}, \dot{\mathbf{y}})^\top \mathbf{J}(\mathbf{x}) \dot{\mathbf{x}}
\end{aligned}$$

When $\mathbf{M}(\mathbf{x}, \dot{\mathbf{x}}) = \mathbf{M}(\mathbf{x})$, $\boldsymbol{\xi}_{\mathbf{M}} = \boldsymbol{\eta}_{\mathbf{M}; \mathcal{S}}$ regardless of the structure of \mathcal{S} .

By Lemma 3, we see that structured GDSs are GDSs regardless of the chosen structure when the metric is only configuration dependent. Thus, the statement of the special case follows by combining Lemma 3 and the previous proof for structured GDSs.

Remarks: Proof of Corollary 1 We note that the non-degenerate assumption does not need to hold for every nodes in RMPflow but only for the root node. This can be seen from the proof above, where we propagate the LHSs and RHSs *separately*. Therefore, as long as the inertial matrix at the root node is invertible, the differential equation on the configuration space is well defined. \blacksquare

Proof of Lemma 2. Let $\mathbf{m}_i, \mathbf{n}_i, \mathbf{j}_i$ be the i th column of \mathbf{M}, \mathbf{N} , and \mathbf{J} , respectively. Suppose \mathcal{M} and \mathcal{N} are of m and n dimensions, respectively. By definition of $\Xi_{\mathbf{M}}$,

$$\begin{aligned}
2\Xi_{\mathbf{M}}(\mathbf{x}, \dot{\mathbf{x}}) &= \sum_{i=1}^m \dot{x}_i \partial_{\dot{\mathbf{x}}} \mathbf{m}_i(\mathbf{x}, \dot{\mathbf{x}}) = \mathbf{J}(\mathbf{x})^\top \sum_{i=1}^m \dot{x}_i \partial_{\dot{\mathbf{x}}} (\mathbf{N}(\mathbf{y}, \dot{\mathbf{y}}) \mathbf{j}_i(\mathbf{x})) \\
&= \mathbf{J}(\mathbf{x})^\top \left(\sum_{i=1}^m \dot{x}_i \partial_{\dot{\mathbf{y}}} (\mathbf{N}(\mathbf{y}, \dot{\mathbf{y}}) \mathbf{j}_i(\mathbf{x})) \right) \mathbf{J}(\mathbf{x}) \\
&= \mathbf{J}(\mathbf{x})^\top \left(\sum_{j=1}^n \partial_{\dot{\mathbf{y}}} \mathbf{n}_j(\mathbf{y}, \dot{\mathbf{y}}) \sum_{i=1}^m \dot{x}_i J_{ji}(\mathbf{x}) \right) \mathbf{J}(\mathbf{x}) \\
&= \mathbf{J}(\mathbf{x})^\top \left(\sum_{j=1}^n y_j \partial_{\dot{\mathbf{y}}} \mathbf{n}_j(\mathbf{y}, \dot{\mathbf{y}}) \right) \mathbf{J}(\mathbf{x}) \\
&= 2\mathbf{J}(\mathbf{x})^\top \Xi_{\mathbf{N}}(\mathbf{y}, \dot{\mathbf{y}}) \mathbf{J}(\mathbf{x}) \quad \blacksquare
\end{aligned}$$

Proof of Lemma 3. Before the proof, we first note a useful identity $\partial_{\dot{\mathbf{x}}} \dot{\mathbf{y}} = \dot{\mathbf{J}}(\mathbf{x}, \dot{\mathbf{x}})$. This can be derived simply by the definition of the Jacobian matrix $(\partial_{\dot{\mathbf{x}}} \mathbf{J}(\mathbf{x}) \dot{\mathbf{x}})_{ij} = \sum_{k=1}^m \dot{x}_k \partial_{x_j} J_{ik} = \sum_{k=1}^m \dot{x}_k \partial_{x_j} \partial_{x_k} y_i = \sum_{k=1}^m \dot{x}_k \partial_{x_k} J_{ij} = (\dot{\mathbf{J}})_{ij}$.

To prove the lemma, we derive $\xi_{\mathbf{M}}$ by its definition

$$\begin{aligned}
\xi_{\mathbf{M}} &= \dot{\mathbf{M}}(\mathbf{x}, \dot{\mathbf{x}}) \dot{\mathbf{x}} - \frac{1}{2} \nabla_{\dot{\mathbf{x}}} (\dot{\mathbf{x}}^\top \mathbf{M}(\mathbf{x}, \dot{\mathbf{x}}) \dot{\mathbf{x}}) \\
&= \dot{\mathbf{J}}(\mathbf{x}, \dot{\mathbf{x}})^\top \mathbf{N}(\mathbf{y}, \dot{\mathbf{y}}) \mathbf{J}(\mathbf{x}) \dot{\mathbf{x}} + \mathbf{J}(\mathbf{x})^\top \mathbf{N}(\mathbf{y}, \dot{\mathbf{y}}) \dot{\mathbf{J}}(\mathbf{x}, \dot{\mathbf{x}}) \dot{\mathbf{x}} + \mathbf{J}(\mathbf{x})^\top \dot{\mathbf{N}}(\mathbf{y}, \dot{\mathbf{y}}) \mathbf{J}(\mathbf{x}) \dot{\mathbf{x}} - \frac{1}{2} \nabla_{\dot{\mathbf{x}}} (\dot{\mathbf{x}}^\top \mathbf{J}(\mathbf{x})^\top \mathbf{N}(\mathbf{y}, \dot{\mathbf{y}}) \mathbf{J}(\mathbf{x}) \dot{\mathbf{x}}) \\
&= \dot{\mathbf{J}}(\mathbf{x}, \dot{\mathbf{x}})^\top \mathbf{N}(\mathbf{y}, \dot{\mathbf{y}}) \dot{\mathbf{y}} + \mathbf{J}(\mathbf{x})^\top \mathbf{N}(\mathbf{y}, \dot{\mathbf{y}}) \dot{\mathbf{J}}(\mathbf{x}, \dot{\mathbf{x}}) \dot{\mathbf{x}} + \mathbf{J}(\mathbf{x})^\top \dot{\mathbf{N}}(\mathbf{y}, \dot{\mathbf{y}}) \dot{\mathbf{y}} - \frac{1}{2} \nabla_{\dot{\mathbf{x}}} (\dot{\mathbf{y}}^\top \mathbf{N}(\mathbf{y}, \dot{\mathbf{y}}) \dot{\mathbf{y}}) \\
&= \dot{\mathbf{J}}(\mathbf{x}, \dot{\mathbf{x}})^\top \mathbf{N}(\mathbf{y}, \dot{\mathbf{y}}) \dot{\mathbf{y}} + \mathbf{J}(\mathbf{x})^\top \mathbf{N}(\mathbf{y}, \dot{\mathbf{y}}) \dot{\mathbf{J}}(\mathbf{x}, \dot{\mathbf{x}}) \dot{\mathbf{x}} + \mathbf{J}(\mathbf{x})^\top \dot{\mathbf{N}}(\mathbf{y}, \dot{\mathbf{y}}) \dot{\mathbf{y}} \\
&\quad - \frac{1}{2} \mathbf{J}(\mathbf{x})^\top \nabla_{\dot{\mathbf{y}}} (\dot{\mathbf{y}}^\top \mathbf{N}(\mathbf{y}, \dot{\mathbf{y}}) \dot{\mathbf{y}}) - \dot{\mathbf{J}}(\mathbf{x}, \dot{\mathbf{x}})^\top \mathbf{N}(\mathbf{y}, \dot{\mathbf{y}}) \dot{\mathbf{y}} - \dot{\mathbf{J}}(\mathbf{x}, \dot{\mathbf{x}})^\top \Xi_{\mathbf{N}}(\mathbf{y}, \dot{\mathbf{y}})^\top \mathbf{J}(\mathbf{x}) \dot{\mathbf{x}} \\
&= \mathbf{J}(\mathbf{x})^\top (\mathbf{N}(\mathbf{y}, \dot{\mathbf{y}}) \dot{\mathbf{J}}(\mathbf{x}, \dot{\mathbf{x}}) \dot{\mathbf{x}} + \dot{\mathbf{N}}(\mathbf{y}, \dot{\mathbf{y}}) \mathbf{J}(\mathbf{x}) \dot{\mathbf{x}} - \frac{1}{2} \nabla_{\dot{\mathbf{y}}} (\dot{\mathbf{y}}^\top \mathbf{N}(\mathbf{y}, \dot{\mathbf{y}}) \dot{\mathbf{y}})) - \dot{\mathbf{J}}(\mathbf{x}, \dot{\mathbf{x}})^\top \Xi_{\mathbf{N}}(\mathbf{y}, \dot{\mathbf{y}})^\top \mathbf{J}(\mathbf{x}) \dot{\mathbf{x}}
\end{aligned}$$

In the second to the last equality above, we use $\partial_{\dot{\mathbf{x}}} \dot{\mathbf{y}} = \dot{\mathbf{J}}(\mathbf{x}, \dot{\mathbf{x}})$ and derive

$$\begin{aligned}
\frac{1}{2} \nabla_{\dot{\mathbf{x}}} (\dot{\mathbf{y}}^\top \mathbf{N}(\mathbf{y}, \dot{\mathbf{y}}) \dot{\mathbf{y}}) &= \frac{1}{2} \mathbf{J}^\top \nabla_{\dot{\mathbf{y}}} (\dot{\mathbf{y}}^\top \mathbf{N}(\mathbf{y}, \dot{\mathbf{y}}) \dot{\mathbf{y}}) + \frac{1}{2} \nabla_{\dot{\mathbf{x}}} (\dot{\mathbf{y}}) \nabla_{\dot{\mathbf{y}}} (\dot{\mathbf{y}}^\top \mathbf{N}(\mathbf{y}, \dot{\mathbf{y}}) \dot{\mathbf{y}}) \\
&= \frac{1}{2} \mathbf{J}^\top \nabla_{\dot{\mathbf{y}}} (\dot{\mathbf{y}}^\top \mathbf{N}(\mathbf{y}, \dot{\mathbf{y}}) \dot{\mathbf{y}}) + \dot{\mathbf{J}}(\mathbf{x}, \dot{\mathbf{x}})^\top \mathbf{N}(\mathbf{y}, \dot{\mathbf{y}}) \dot{\mathbf{y}} + \frac{1}{2} \dot{\mathbf{J}}(\mathbf{x}, \dot{\mathbf{x}})^\top \nabla_{\dot{\mathbf{y}}} (\mathbf{z}^\top \mathbf{N}(\mathbf{y}, \dot{\mathbf{y}}) \dot{\mathbf{z}}) \Big|_{\mathbf{z}=\dot{\mathbf{y}}} \\
&= \frac{1}{2} \mathbf{J}^\top \nabla_{\dot{\mathbf{y}}} (\dot{\mathbf{y}}^\top \mathbf{N}(\mathbf{y}, \dot{\mathbf{y}}) \dot{\mathbf{y}}) + \dot{\mathbf{J}}(\mathbf{x}, \dot{\mathbf{x}})^\top \mathbf{N}(\mathbf{y}, \dot{\mathbf{y}}) \dot{\mathbf{y}} + \dot{\mathbf{J}}(\mathbf{x}, \dot{\mathbf{x}})^\top \Xi_{\mathbf{N}}(\mathbf{y}, \dot{\mathbf{y}})^\top \mathbf{J}(\mathbf{x}) \dot{\mathbf{x}}
\end{aligned}$$

as $\frac{1}{2} \partial_{\dot{\mathbf{y}}} (\mathbf{z}^\top \mathbf{N}(\mathbf{y}, \dot{\mathbf{y}}) \dot{\mathbf{z}}) \Big|_{\mathbf{z}=\dot{\mathbf{y}}} = \frac{1}{2} \dot{\mathbf{y}}^\top (\sum_{i=1}^n \dot{y}_i \partial_{\dot{\mathbf{y}}} \mathbf{n}_i(\mathbf{y}, \dot{\mathbf{y}})) = \dot{\mathbf{y}}^\top \Xi_{\mathbf{N}}(\mathbf{y}, \dot{\mathbf{y}})$, where \mathbf{n}_i is the i th column of \mathbf{N} .

To further simplify the expression, we note that by $\partial_{\dot{\mathbf{x}}}\dot{\mathbf{y}} = \dot{\mathbf{J}}(\mathbf{x}, \dot{\mathbf{x}})$ we have

$$\begin{aligned}
\dot{\mathbf{N}}(\mathbf{y}, \dot{\mathbf{y}})\dot{\mathbf{y}} &= \sum_{i=1}^n \dot{y}_i \partial_{\dot{\mathbf{x}}}\mathbf{n}_i(\mathbf{y}, \dot{\mathbf{y}})\dot{\mathbf{x}} \\
&= \sum_{i=1}^n \dot{y}_i (\partial_{\mathbf{y}}\mathbf{n}_i(\mathbf{y}, \dot{\mathbf{y}})\mathbf{J}(\mathbf{x})\dot{\mathbf{x}} + \partial_{\dot{\mathbf{y}}}\mathbf{n}_i(\mathbf{y}, \dot{\mathbf{y}})\partial_{\dot{\mathbf{x}}}(\dot{\mathbf{y}})\dot{\mathbf{x}}) \\
&= \sum_{i=1}^n \dot{y}_i \partial_{\mathbf{y}}\mathbf{n}_i(\mathbf{y}, \dot{\mathbf{y}})\dot{\mathbf{y}} + \dot{y}_i \partial_{\dot{\mathbf{y}}}\mathbf{n}_i(\mathbf{y}, \dot{\mathbf{y}})\dot{\mathbf{J}}(\mathbf{x}, \dot{\mathbf{x}})\dot{\mathbf{x}} \\
&= \left(\sum_{i=1}^n \dot{y}_i \partial_{\mathbf{y}}\mathbf{n}_i(\mathbf{y}, \dot{\mathbf{y}}) \right) \dot{\mathbf{y}} + \left(\sum_{i=1}^n \dot{y}_i \partial_{\dot{\mathbf{y}}}\mathbf{n}_i(\mathbf{y}, \dot{\mathbf{y}}) \right) \dot{\mathbf{J}}(\mathbf{x}, \dot{\mathbf{x}})\dot{\mathbf{x}} \\
&= \dot{\mathbf{N}}(\mathbf{y}, \dot{\mathbf{y}})\dot{\mathbf{y}} + 2\Xi_{\mathbf{N}}(\mathbf{y}, \dot{\mathbf{y}})\dot{\mathbf{J}}(\mathbf{x}, \dot{\mathbf{x}})\dot{\mathbf{x}}
\end{aligned}$$

Combining these two equalities, we can write

$$\begin{aligned}
\xi_{\mathbf{M}}(\mathbf{x}, \dot{\mathbf{x}}) &= \mathbf{J}(\mathbf{x})^\top \left(\dot{\mathbf{N}}(\mathbf{y}, \dot{\mathbf{y}})\dot{\mathbf{y}} - \frac{1}{2}\nabla_{\dot{\mathbf{y}}}(\dot{\mathbf{y}}^\top \mathbf{N}(\mathbf{y}, \dot{\mathbf{y}})\dot{\mathbf{y}}) + (\mathbf{N}(\mathbf{y}, \dot{\mathbf{y}}) + 2\Xi_{\mathbf{N}}(\mathbf{y}, \dot{\mathbf{y}}))\dot{\mathbf{J}}(\mathbf{x}, \dot{\mathbf{x}})\dot{\mathbf{x}} \right) \\
&\quad - \dot{\mathbf{J}}(\mathbf{x}, \dot{\mathbf{x}})^\top \Xi_{\mathbf{N}}(\mathbf{y}, \dot{\mathbf{y}})^\top \mathbf{J}(\mathbf{x})\dot{\mathbf{x}}
\end{aligned}$$

Substituting the definition of $\xi_{\mathbf{N}}(\mathbf{y}, \dot{\mathbf{y}}) = \dot{\mathbf{N}}(\mathbf{y}, \dot{\mathbf{y}})\dot{\mathbf{y}} - \frac{1}{2}\nabla_{\dot{\mathbf{y}}}(\dot{\mathbf{y}}^\top \mathbf{N}(\mathbf{y}, \dot{\mathbf{y}})\dot{\mathbf{y}})$ proves the general statement.

In the special case, $\mathbf{M}(\mathbf{x}, \dot{\mathbf{x}}) = \mathbf{M}(\mathbf{x})$ (which implies $\Xi_{\mathbf{M}} = 0$),

$$\xi_{\mathbf{M}}(\mathbf{x}, \dot{\mathbf{x}}) = \mathbf{J}(\mathbf{x})^\top \left(\xi_{\mathbf{N}}(\mathbf{y}, \dot{\mathbf{y}}) + \mathbf{N}(\mathbf{y})\dot{\mathbf{J}}(\mathbf{x}, \dot{\mathbf{x}})\dot{\mathbf{x}} \right)$$

We show this expression is equal to $\eta_{\mathbf{M};\mathcal{S}}$ regardless of the structure \mathcal{S} . This can be seen from the follows: If further $\mathbf{N}(\mathbf{y}) = \mathbf{L}(\mathbf{y})^\top \mathbf{C}(\mathbf{z})\mathbf{L}(\mathbf{y})$ and \mathbf{M} is structured as $(\mathbf{L}\mathbf{J})^\top \mathbf{C}(\mathbf{L}\mathbf{J})$ from some Jacobian matrix $\mathbf{L}(\mathbf{y}) = \partial_{\mathbf{y}}\mathbf{z}$, we can write

$$\begin{aligned}
\eta_{\mathbf{M};\mathcal{S}} &= \mathbf{J}^\top \mathbf{L}^\top \left(\xi_{\mathbf{C}} + \mathbf{C} \frac{d(\mathbf{L}\mathbf{J})}{dt} \dot{\mathbf{x}} \right) \\
&= \mathbf{J}^\top \left(\mathbf{L}^\top \xi_{\mathbf{C}} + \mathbf{L}^\top \mathbf{C}(\dot{\mathbf{L}}\mathbf{J} + \mathbf{L}\dot{\mathbf{J}})\dot{\mathbf{x}} \right) \\
&= \mathbf{J}^\top \left(\mathbf{L}^\top (\xi_{\mathbf{C}} + \mathbf{C}\dot{\mathbf{L}}\dot{\mathbf{y}}) + \mathbf{L}^\top \mathbf{C}\mathbf{L}\dot{\mathbf{J}}\dot{\mathbf{x}} \right) \\
&= \mathbf{J}^\top \left(\xi_{\mathbf{N}} + \mathbf{N}\dot{\mathbf{J}}\dot{\mathbf{x}} \right) = \xi_{\mathbf{M}} \quad \blacksquare
\end{aligned}$$

B.2 Proof of Proposition 1

Proposition 1. For $(\mathcal{C}, \mathbf{G}, \mathbf{B}, \Phi)_{\mathcal{S}}$, $\dot{\mathbf{V}}(\mathbf{q}, \dot{\mathbf{q}}) = -\dot{\mathbf{q}}^\top \mathbf{B}(\mathbf{q}, \dot{\mathbf{q}})\dot{\mathbf{q}}$.

Proof of Proposition 1. Let $K(\mathbf{q}, \dot{\mathbf{q}}) = \frac{1}{2} \dot{\mathbf{q}}^\top \mathbf{G}(\mathbf{q}, \dot{\mathbf{q}}) \dot{\mathbf{q}}$. Its time derivative can be written as

$$\begin{aligned} \frac{d}{dt} K(\mathbf{q}, \dot{\mathbf{q}}) &= \dot{\mathbf{q}}^\top \left(\mathbf{G}(\mathbf{q}, \dot{\mathbf{q}}) \ddot{\mathbf{q}} + \frac{1}{2} \left(\frac{d}{dt} \mathbf{G}(\mathbf{q}, \dot{\mathbf{q}}) \right) \dot{\mathbf{q}} \right) \\ &= \dot{\mathbf{q}}^\top \left(\mathbf{G}(\mathbf{q}, \dot{\mathbf{q}}) \ddot{\mathbf{q}} + \frac{1}{2} \sum_{i=1}^d \dot{q}_i \frac{d}{dt} \mathbf{g}_i(\mathbf{q}, \dot{\mathbf{q}}) \right) \\ &= \dot{\mathbf{q}}^\top \left(\mathbf{G}(\mathbf{q}, \dot{\mathbf{q}}) \ddot{\mathbf{q}} + \frac{1}{2} \sum_{i=1}^d \dot{q}_i \partial_{\mathbf{q}} \mathbf{g}_i(\mathbf{q}, \dot{\mathbf{q}}) \dot{\mathbf{q}} + \frac{1}{2} \sum_{i=1}^d \dot{q}_i \partial_{\dot{\mathbf{q}}} \mathbf{g}_i(\mathbf{q}, \dot{\mathbf{q}}) \ddot{\mathbf{q}} \right) \\ &= \dot{\mathbf{q}}^\top \left((\mathbf{G}(\mathbf{q}, \dot{\mathbf{q}}) + \Xi_{\mathbf{G}}(\mathbf{q}, \dot{\mathbf{q}})) \ddot{\mathbf{q}} + \frac{1}{2} \overset{\mathbf{a}}{\mathbf{G}}(\mathbf{q}, \dot{\mathbf{q}}) \dot{\mathbf{q}} \right) \end{aligned}$$

where we recall \mathbf{G} is symmetric and $\overset{\mathbf{a}}{\mathbf{G}}(\mathbf{q}, \dot{\mathbf{q}}) := [\partial_{\mathbf{q}} \mathbf{g}_i(\mathbf{q}, \dot{\mathbf{q}}) \dot{q}_i]_{i=1}^d$. Therefore, by definition $(\mathbf{G}(\mathbf{q}, \dot{\mathbf{q}}) + \Xi_{\mathbf{G}}(\mathbf{q}, \dot{\mathbf{q}})) \ddot{\mathbf{q}} = (-\boldsymbol{\eta}_{\mathbf{G};S}(\mathbf{q}, \dot{\mathbf{q}}) - \nabla_{\mathbf{q}} \Phi(\mathbf{q}) - \mathbf{B}(\mathbf{q}, \dot{\mathbf{q}}) \dot{\mathbf{x}}(\mathbf{q}, \dot{\mathbf{q}}))$, we can derive

$$\begin{aligned} \frac{d}{dt} \mathbf{V}(\mathbf{q}, \dot{\mathbf{q}}) &= \frac{d}{dt} K(\mathbf{q}, \dot{\mathbf{q}}) + \dot{\mathbf{q}}^\top \nabla_{\mathbf{q}} \Phi(\mathbf{q}) \\ &= \dot{\mathbf{q}}^\top \left(-\boldsymbol{\eta}_{\mathbf{G};S}(\mathbf{q}, \dot{\mathbf{q}}) - \nabla_{\mathbf{q}} \Phi(\mathbf{q}) - \mathbf{B}(\mathbf{q}, \dot{\mathbf{q}}) \dot{\mathbf{x}} + \frac{1}{2} \overset{\mathbf{a}}{\mathbf{G}}(\mathbf{q}, \dot{\mathbf{q}}) \dot{\mathbf{q}} + \nabla_{\mathbf{q}} \Phi(\mathbf{q}) \right) \\ &= -\dot{\mathbf{q}}^\top \mathbf{B}(\mathbf{q}, \dot{\mathbf{q}}) \dot{\mathbf{x}} + \dot{\mathbf{q}}^\top \left(-\boldsymbol{\eta}_{\mathbf{G};S}(\mathbf{q}, \dot{\mathbf{q}}) + \frac{1}{2} \overset{\mathbf{a}}{\mathbf{G}}(\mathbf{q}, \dot{\mathbf{q}}) \dot{\mathbf{q}} \right) \end{aligned}$$

To finish the proof, we use two lemmas below.

Lemma 4. $\frac{1}{2} \dot{\mathbf{q}}^\top \overset{\mathbf{a}}{\mathbf{G}}(\mathbf{q}, \dot{\mathbf{q}}) \dot{\mathbf{q}} = \dot{\mathbf{q}}^\top \boldsymbol{\xi}_{\mathbf{G}}(\mathbf{q}, \dot{\mathbf{q}})$.

Proof of Lemma 4. This can be shown by definition:

$$\begin{aligned} \dot{\mathbf{q}}^\top \boldsymbol{\xi}_{\mathbf{G}}(\mathbf{q}, \dot{\mathbf{q}}) &= \dot{\mathbf{q}}^\top \left(\overset{\mathbf{a}}{\mathbf{G}}(\mathbf{q}, \dot{\mathbf{q}}) \dot{\mathbf{q}} - \frac{1}{2} \nabla_{\mathbf{q}} (\dot{\mathbf{q}}^\top \mathbf{G}(\mathbf{q}, \dot{\mathbf{q}}) \dot{\mathbf{q}}) \right) \\ &= \sum_{k=1}^d \dot{q}_k \left(\sum_{i,j=1}^d \dot{q}_i \dot{q}_j \partial_{q_j} G_{k,i} - \frac{1}{2} \sum_{i,j=1}^d \dot{q}_i \dot{q}_j \partial_{q_k} G_{i,j} \right) \\ &= \sum_{i,j,k=1}^d \dot{q}_i \dot{q}_j \dot{q}_k \partial_{q_j} G_{k,i} - \frac{1}{2} \sum_{i,j,k=1}^d \dot{q}_i \dot{q}_j \dot{q}_k \partial_{q_k} G_{i,j} \\ &= \sum_{i,j,k=1}^d \dot{q}_i \dot{q}_j \dot{q}_k \partial_{q_k} G_{j,i} - \frac{1}{2} \sum_{i,j,k=1}^d \dot{q}_i \dot{q}_j \dot{q}_k \partial_{q_k} G_{i,j} \\ &= \frac{1}{2} \sum_{i,j,k=1}^d \dot{q}_i \dot{q}_j \dot{q}_k \partial_{q_j} G_{k,i} = \frac{1}{2} \dot{\mathbf{q}}^\top \overset{\mathbf{a}}{\mathbf{G}}(\mathbf{q}, \dot{\mathbf{q}}) \dot{\mathbf{q}} \end{aligned}$$

where for the second to the last equality we use the symmetry $G_{i,j} = G_{j,i}$. \blacksquare

Using Lemma 4, we can show another equality.

Lemma 5. For all structure \mathcal{S} , $\dot{\mathbf{q}}^\top \left(-\boldsymbol{\eta}_{\mathcal{G};\mathcal{S}}(\mathbf{q}, \dot{\mathbf{q}}) + \frac{1}{2} \mathring{\mathbf{G}}(\mathbf{q}, \dot{\mathbf{q}}) \dot{\mathbf{q}} \right) = 0$

Proof of Lemma 5. This can be seen from Lemma 3. Suppose \mathcal{S} factorizes $\mathbf{G}(\mathbf{q}, \dot{\mathbf{q}}) = \mathbf{J}(\mathbf{q})^\top \mathbf{H}(\mathbf{x}, \dot{\mathbf{x}}) \mathbf{J}(\mathbf{q})$ where $\mathbf{J}(\mathbf{q}) = \partial_{\mathbf{q}} \mathbf{x}$. By Lemma 3, we know

$$\boldsymbol{\xi}_{\mathbf{G}} = \mathbf{J}^\top \left(\boldsymbol{\xi}_{\mathbf{H}} + (\mathbf{H} + 2\boldsymbol{\Xi}_{\mathbf{H}}) \mathbf{J} \dot{\mathbf{x}} \right) - \dot{\mathbf{J}}^\top \boldsymbol{\Xi}_{\mathbf{H}}^\top \mathbf{J} \dot{\mathbf{x}}$$

On the other hand, by definition, we have $\boldsymbol{\eta}_{\mathcal{G};\mathcal{S}} := \mathbf{J}^\top (\boldsymbol{\xi}_{\mathbf{H}} + (\mathbf{H} + \boldsymbol{\Xi}_{\mathbf{H}}) \mathbf{J} \dot{\mathbf{x}})$. Therefore, by comparing the two, we can derive,

$$\dot{\mathbf{q}}^\top \boldsymbol{\xi}_{\mathbf{G}} = \dot{\mathbf{q}}^\top \left(\boldsymbol{\eta}_{\mathcal{G};\mathcal{S}} + \mathbf{J}^\top \boldsymbol{\Xi}_{\mathbf{H}} \mathbf{J} \dot{\mathbf{q}} - \dot{\mathbf{J}}^\top \boldsymbol{\Xi}_{\mathbf{H}}^\top \mathbf{J} \dot{\mathbf{q}} \right) = \dot{\mathbf{q}}^\top \boldsymbol{\eta}_{\mathcal{G};\mathcal{S}}$$

Combing the above equality and Lemma 4 proves the equality. \blacksquare

Finally, we use Lemma 5 and the previous result and conclude

$$\frac{d}{dt} \mathbf{V}(\mathbf{q}, \dot{\mathbf{q}}) = -\dot{\mathbf{q}}^\top \mathbf{B}(\mathbf{q}, \dot{\mathbf{q}}) \dot{\mathbf{q}} + \dot{\mathbf{q}}^\top \left(-\boldsymbol{\eta}_{\mathcal{G};\mathcal{S}}(\mathbf{q}, \dot{\mathbf{q}}) + \frac{1}{2} \mathring{\mathbf{G}}(\mathbf{q}, \dot{\mathbf{q}}) \dot{\mathbf{q}} \right) = -\dot{\mathbf{q}}^\top \mathbf{B}(\mathbf{q}, \dot{\mathbf{q}}) \dot{\mathbf{q}} \blacksquare$$

B.3 Proof of Theorem 2

Theorem 2. Suppose every leaf node is a GDS with a metric matrix in the form $\mathbf{R}(\mathbf{x}) + \mathbf{L}(\mathbf{x})^\top \mathbf{D}(\mathbf{x}, \dot{\mathbf{x}}) \mathbf{L}(\mathbf{x})$ for differentiable functions \mathbf{R} , \mathbf{L} , and \mathbf{D} satisfying $\mathbf{R}(\mathbf{x}) \succeq 0$, $\mathbf{D}(\mathbf{x}, \dot{\mathbf{x}}) = \text{diag}((d_i(\mathbf{x}, \dot{y}_i))_{i=1}^n) \succeq 0$, and $\dot{y}_i \partial_{\dot{y}_i} d_i(\mathbf{x}, \dot{y}_i) \geq 0$, where \mathbf{x} is the coordinate of the leaf-node manifold and $\dot{\mathbf{y}} = \mathbf{L} \dot{\mathbf{x}} \in \mathbb{R}^n$. It holds $\boldsymbol{\Xi}_{\mathbf{G}}(\mathbf{q}, \dot{\mathbf{q}}) \succeq 0$. If further $\mathbf{G}(\mathbf{q}, \dot{\mathbf{q}}), \mathbf{B}(\mathbf{q}, \dot{\mathbf{q}}) \succ 0$, then $\mathbf{M} \in \mathbb{R}_{++}^{d \times d}$, and the global RMP generated by RMPflow converges to the forward invariant set \mathcal{C}_∞ in Corollary 2.

Proof. Let $\mathbf{A}(\mathbf{x}, \dot{\mathbf{x}}) = \mathbf{R}(\mathbf{x}) + \mathbf{L}(\mathbf{x})^\top \mathbf{D}(\mathbf{x}, \dot{\mathbf{x}}) \mathbf{L}(\mathbf{x})$. The proof of the theorem is straightforward, if we show that $\boldsymbol{\Xi}_{\mathbf{A}}(\mathbf{x}, \dot{\mathbf{x}}) \succeq 0$. To see this, suppose $\mathbf{L} = \mathbb{R}^{n \times m}$. Let $\boldsymbol{\omega}_j^\top$ be the j th row \mathbf{L} , respectively. By definition of $\boldsymbol{\Xi}_{\mathbf{A}}(\mathbf{x}, \dot{\mathbf{x}})$ we can write

$$\begin{aligned} \boldsymbol{\Xi}_{\mathbf{A}}(\mathbf{x}, \dot{\mathbf{x}}) &= \frac{1}{2} \sum_{i=1}^m \dot{x}_i \partial_{\dot{\mathbf{x}}} \mathbf{a}_i(\mathbf{x}, \dot{\mathbf{x}}) \\ &= \frac{1}{2} \mathbf{L}(\mathbf{x})^\top \sum_{i=1}^m \dot{x}_i \partial_{\dot{\mathbf{x}}} (\mathbf{D}(\mathbf{x}, \dot{\mathbf{x}}) \mathbf{l}_i(\mathbf{x})) \\ &= \frac{1}{2} \mathbf{L}(\mathbf{x})^\top \sum_{i=1}^m \sum_{j=1}^n \dot{x}_i \partial_{\dot{\mathbf{x}}} (d_j(\mathbf{x}, \dot{y}_j) L_{ji}(\mathbf{x}) \mathbf{e}_j) \\ &= \frac{1}{2} \mathbf{L}(\mathbf{x})^\top \sum_{j=1}^n \left(\sum_{i=1}^m L_{ji}(\mathbf{x}) \dot{x}_i \right) \partial_{\dot{y}_j} d_j(\mathbf{x}, \dot{y}_j) \mathbf{e}_j \boldsymbol{\omega}_j^\top \\ &= \frac{1}{2} \mathbf{L}(\mathbf{x})^\top \sum_{j=1}^n \dot{y}_j \partial_{\dot{y}_j} d_j(\mathbf{x}, \dot{y}_j) \mathbf{e}_j \boldsymbol{\omega}_j^\top \\ &= \mathbf{L}(\mathbf{x})^\top \boldsymbol{\Xi}_{\mathbf{D}}(\mathbf{x}, \dot{\mathbf{x}}) \mathbf{L}(\mathbf{x}) \end{aligned}$$

where \mathbf{e}_j the j th canonical basis and $\Xi_D(\mathbf{x}, \dot{\mathbf{x}}) = \frac{1}{2} \text{diag}((\partial_{y_i} d_i(\mathbf{x}, \dot{y}_i))_{i=1}^n)$. Therefore, under the assumption that $\partial_{y_i} d_i(\mathbf{x}, \dot{y}_i) \geq 0$, $\Xi_A(\mathbf{x}, \dot{\mathbf{x}}) \succeq 0$. This further implies $\Xi_G(\mathbf{q}, \dot{\mathbf{q}}) \succeq 0$ by Theorem 1.

The stability of the entire system follows naturally from the rule of **pullback**, which ensures that $\mathbf{M}_r(\mathbf{q}, \dot{\mathbf{q}}) = \mathbf{M}(\mathbf{q}, \dot{\mathbf{q}}) = \mathbf{G}(\mathbf{q}, \dot{\mathbf{q}}) + \Xi_G(\mathbf{q}, \dot{\mathbf{q}}) \succ 0$ given that the leaf-node condition is satisfied. Consequently, the condition in Corollary 2 holds and the convergence to \mathcal{C}_∞ is guaranteed. \blacksquare

B.4 Notation for Coordinate-Free Analysis

We introduce some extra notations for the coordinate-free analysis. Let $p_{TC} : TC \rightarrow \mathcal{C}$ be the bundle projection. Suppose $(U, (\mathbf{q}, \mathbf{v}))$ is a (local) chart on TC . Let $\{\frac{\partial}{\partial q_i}, \frac{\partial}{\partial v_i}\}_{i=1}^d$ and $\{dq^i, dv^i\}_{i=1}^d$ denote the induced frame field and coframe field on TC . For $s \in U$, we write s in coordinate as $(\mathbf{q}(q), \mathbf{v}(s))$, if $\sum_{i=1}^d v_i(s) \frac{\partial}{\partial q_i}|_q \in T_q \mathcal{C}$, where $q = p_{TC}(s) \in \mathcal{C}$. With abuse of notation, we also write $s = (\mathbf{q}, \mathbf{v})$ for short unless clarity is lost. Similarly, a chart $(\tilde{U}, (\mathbf{q}, \mathbf{v}, \mathbf{u}, \mathbf{a}))$ can naturally be constructed on the double tangent bundle TTC , where $\tilde{U} = p_{TTC}^{-1}(U)$ and $p_{TTC} : TTC \rightarrow TC$ is the bundle projection: we write $h = (\mathbf{q}, \mathbf{v}, \mathbf{u}, \mathbf{a}) \in TTC$ if $\sum_{i=1}^d u_i(h) \frac{\partial}{\partial q_i}|_s + a_i(h) \frac{\partial}{\partial v_i}|_s \in T_s TC$, where $s = p_{TTC}(h)$. Under these notations, for a curve $q(t)$ on \mathcal{C} , we can write $\dot{q}(t) \in TTC$ in coordinate as $(\mathbf{q}(t), \dot{\mathbf{q}}(t), \dot{\mathbf{q}}(t), \ddot{\mathbf{q}}(t))$. Finally, given Christoffel symbols $\Gamma_{i,j}^k$, an affine connection ∇ on TTC is defined via $\nabla_{\frac{\partial}{\partial s_i}} \frac{\partial}{\partial s_j} = \sum_{k=1}^{2d} \Gamma_{i,j}^k \frac{\partial}{\partial s_k}$, where $\frac{\partial}{\partial s_i} := \frac{\partial}{\partial q_i}$ and $\frac{\partial}{\partial s_{i+d}} := \frac{\partial}{\partial v_i}$ for $i = 1, \dots, d$.

B.5 Proof of Theorem 3

Theorem 3. *Let G be a Riemannian metric on TC such that, for $s = (q, v) \in TC$, $G(s) = G_{ij}^v(s) dq^i \otimes dq^j + G_{ij}^a dv^i \otimes dv^j$, where $G_{ij}^v(s)$ and G_{ij}^a are symmetric and positive-definite, and $G_{ij}^v(\cdot)$ is differentiable. Then there is a unique affine connection ${}^G\nabla$ that is compatible with G and satisfies, $\Gamma_{i,j}^k = \Gamma_{j,i}^k$, $\Gamma_{i,j+d}^k = 0$, and $\Gamma_{i+d,j+d}^k = \Gamma_{j+d,i+d}^k$, for $i, j = 1, \dots, d$ and $k = 1, \dots, 2d$. In coordinates, if $G_{ij}^v(\dot{q})$ is identified as $\mathbf{G}(\mathbf{q}, \dot{\mathbf{q}})$, then $\text{pr}_3({}^G\nabla_{\dot{q}} \ddot{q})$ can be written as $\mathbf{a}_G := \ddot{\mathbf{q}} + \mathbf{G}(\mathbf{q}, \dot{\mathbf{q}})^{-1}(\xi_G(\mathbf{q}, \dot{\mathbf{q}}) + \Xi_G(\mathbf{q}, \dot{\mathbf{q}})\ddot{\mathbf{q}})$, where $\text{pr}_3 : (\mathbf{q}, \mathbf{v}, \mathbf{u}, \mathbf{a}) \mapsto \mathbf{u}$ is a projection.*

Proof of Theorem 3. We first show ${}^G\nabla$ is unique, if it exists. That is, there is at most one affine connection that is compatible with the given the Riemannian metric G and satisfies for $i, j = 1, \dots, d$ and $k = 1, \dots, 2d$

$$\Gamma_{i,j}^k = \Gamma_{j,i}^k, \quad \Gamma_{i,j+d}^k = 0, \quad \Gamma_{i+d,j+d}^k = \Gamma_{j+d,i+d}^k,$$

Importantly, we note that this definition is coordinate-free, independent of the choice of chart on \mathcal{C} .

The uniqueness is easy to see. As G is non-degenerate by definition, we recall there is an unique Levi-Civita connection, which is compatible with G and

satisfies the symmetric condition

$$\Gamma_{i,j}^k = \Gamma_{j,i}^k, \quad \text{for } i, j = 1, \dots, 2d$$

Comparing our asymmetric condition and the symmetric condition of the Levi-Civita connection, we see that number of the linearly independent constraints are the same; therefore if there is a solution to the required asymmetric affine connection, then it is unique.

Next we show such a solution exists. We consider the candidate Christoffel symbols below and show that they satisfy the requirements: Consider an *arbitrary* choice of chart on \mathcal{C} . For $i, j, k = 1, \dots, d$,

$$\begin{aligned} \Gamma_{i,j}^k &= \frac{1}{2} \sum_{l=1}^d G_{k,l}^{v\sharp} (\partial_{q_j} G_{l,i}^v + \partial_{q_i} G_{l,j}^v - \partial_{q_l} G_{i,j}^v) \\ \Gamma_{i,j+d}^k &= 0, \quad \Gamma_{i+d,j}^k = \frac{1}{2} \sum_{l=1}^d G_{k,l}^{v\sharp} (\partial_{v_i} G_{l,j}^v), \quad \Gamma_{i+d,j+d}^k = 0 \\ \Gamma_{i,j}^{k+d} &= 0, \quad \Gamma_{i,j+d}^{k+d} = 0, \quad \Gamma_{i+d,j}^{k+d} = 0, \quad \Gamma_{i+d,j+d}^{k+d} = 0 \end{aligned}$$

where $G^{v\sharp}$ denotes the inverse of G^v , i.e. $\sum_{k=1}^d G_{i,k}^{v\sharp} G_{k,j}^v = \delta_{i,j}$. Note we choose not to adopt the Einstein summation notation, so the sparse pattern of the proposed Christoffel symbols are clear.

It is clear that the above candidate Christoffel symbols satisfies the asymmetric condition. Therefore, to show it is a solution, we only need to show such choice is compatible with G . Equivalently, it means for arbitrary smooth sections of TTC , $X = \sum_{i=1}^{2d} X_i \frac{\partial}{\partial s_i}$, $Y = \sum_{i=1}^{2d} Y_i \frac{\partial}{\partial s_i}$, $Z = \sum_{i=1}^{2d} Z_i \frac{\partial}{\partial s_i}$, it holds⁹

$${}^G \nabla_Z G(X, Y) = G({}^G \nabla_Z X, Y) + G(X, {}^G \nabla_Z Y) \quad (8)$$

To verify (8), we first write out ${}^G \nabla_Z X$ using the chosen Christoffel symbols:

$$\begin{aligned} {}^G \nabla_Z X &= \sum_{k=1}^{2d} \left({}^G \nabla_Z X_k + \sum_{i,j=1}^{2d} \Gamma_{ij}^k Z_i X_j \right) \frac{\partial}{\partial s_k} \\ &= \sum_{k=1}^d D_Z(X_k) \frac{\partial}{\partial q_k} + \sum_{k=1}^d D_Z(X_{k+d}) \frac{\partial}{\partial v_k} \\ &\quad + \frac{1}{2} \sum_{k,l=1}^d G^{v,kl} \left(\sum_{i,j=1}^d (\partial_{q_j} G_{li}^v + \partial_{q_i} G_{lj}^v - \partial_{q_l} G_{ij}^v) Z_i X_j + (\partial_{v_i} G_{lj}^v) Z_{i+d} X_j \right) \frac{\partial}{\partial q_k} \end{aligned} \quad (9)$$

⁹ The section requirement on Z can be dropped.

where $D_Z(\cdot)$ denotes the derivation with respect to Z . The above implies

$$\begin{aligned} G({}^G\nabla_Z X, Y) &= \sum_{j,k=1}^d G_{ki}^v Y_k D_Z(X_i) + \sum_{j,k=1}^d G_{kj}^a Y_{k+d} D_Z(X_{j+d}) \\ &\quad + \frac{1}{2} \left(\sum_{i,j,k=1}^d (\partial_{q_j} G_{ki}^v + \partial_{q_i} G_{kj}^v - \partial_{q_k} G_{ij}^v) Z_i X_j Y_k + (\partial_{v_i} G_{kj}^v) Z_{i+d} X_j Y_k \right) \end{aligned}$$

Similarly, we can derive $G(X, {}^G\nabla_Z Y)$. Using the symmetry $G_{ij}^v = G_{ji}^v$, we can combine the previous results together and write

$$\begin{aligned} &G({}^G\nabla_Z X, Y) + G(X, {}^G\nabla_Z Y) \\ &= \sum_{j,k=1}^d G_{ki}^v Y_k D_Z(X_i) + \sum_{j,k=1}^d G_{kj}^a Y_{k+d} D_Z(X_{j+d}) + \sum_{j,k=1}^d G_{ki}^v X_k D_Z(Y_i) + \sum_{j,k=1}^d G_{kj}^a X_{k+d} D_Z(Y_{j+d}) \\ &\quad + \frac{1}{2} \left(\sum_{i,j,k=1}^d (\partial_{q_j} G_{ki}^v + \partial_{q_i} G_{kj}^v - \partial_{q_k} G_{ij}^v) Z_i X_j Y_k + (\partial_{v_i} G_{kj}^v) Z_{i+d} X_j Y_k \right) \\ &\quad + \frac{1}{2} \left(\sum_{i,j,k=1}^d (\partial_{q_j} G_{ki}^v + \partial_{q_i} G_{kj}^v - \partial_{q_k} G_{ij}^v) Z_i Y_j X_k + (\partial_{v_i} G_{kj}^v) Z_{i+d} Y_j X_k \right) \\ &= \sum_{i,j=1}^d G_{ij}^v D_Z(X_i) Y_j + G_{ij}^v X_i D_Z(Y_j) + \sum_{i,j=1}^d G_{ij}^a D_Z(X_{d+i}) Y_{d+j} + G_{ij}^a X_{d+i} D_Z(Y_{d+j}) \\ &\quad + \sum_{i,j,k=1}^d X_i Y_j Z_k \partial_{q_k} G_{ij}^v + X_i Y_j Z_{k+d} \partial_{v_k} G_{ij}^v \\ &= \sum_{i,j=1}^d D_Z(G_{ij}^v) X_i Y_j + G_{ij}^v D_Z(X_i) Y_j + G_{ij}^v X_i D_Z(Y_j) + \sum_{i,j=1}^d G_{ij}^a D_Z(X_{d+i}) Y_{d+j} + G_{ij}^a X_{d+i} D_Z(Y_{d+j}) \\ &= {}^G\nabla_Z \left(\sum_{i,j=1}^d G_{ij}^v X_i Y_j + \sum_{i,j=1}^d G_{ij}^a X_{d+i} Y_{d+j} \right) = {}^G\nabla_Z G(X, Y) \end{aligned}$$

Therefore ${}^G\nabla$ is compatible with G .

So far we have proved the first statement of Theorem 3 that ${}^G\nabla$ is the unique solution that is compatible with G and satisfies the asymmetric condition. Below we show the expression of $\text{pr}_3({}^G\nabla_{\dot{q}}\dot{q})$, where we recall $\dot{q}(t)$ is a curve in TTC . We use (9). By definition of pr_3 it extracts the parts on $\{\frac{\partial}{\partial q_i}\}_{i=1}^d$. Therefore,

suppose we choose some chart on \mathcal{C} of interest and we can write $\text{pr}_3({}^G\nabla_{\ddot{q}}\ddot{q})$ as

$$\begin{aligned}\text{pr}_3({}^G\nabla_{\ddot{q}}\ddot{q}) &= \sum_k^d \left(D_Z(X_k) + \sum_{l=1}^d \frac{1}{2} G^{v,kl} \sum_{i,j=1}^d (\partial_{q_j} G_{li}^v + \partial_{q_i} G_{lj}^v - \partial_{q_l} G_{ij}^v) Z_i X_j + (\partial_{v_i} G_{lj}^v) Z_{i+d} X_j \right) \frac{\partial}{\partial q_k} \\ &= \sum_k^d \left(\ddot{q}_k + \sum_{l=1}^d \frac{1}{2} G^{v,kl} \sum_{i,j=1}^d (\partial_{q_j} G_{li}^v + \partial_{q_i} G_{lj}^v - \partial_{q_l} G_{ij}^v) \dot{q}_i \dot{q}_j + (\partial_{v_i} G_{lj}^v) \ddot{q}_i \dot{q}_j \right) \frac{\partial}{\partial q_k} \\ &= \sum_k^d a_{\mathbf{G};k} \frac{\partial}{\partial q_k}\end{aligned}$$

where $a_{\mathbf{G};k}$ is the k th element of $\mathbf{a}_{\mathbf{G}} := \ddot{\mathbf{q}} + \mathbf{G}(\mathbf{q}, \dot{\mathbf{q}})^{-1} (\boldsymbol{\xi}_{\mathbf{G}}(\mathbf{q}, \dot{\mathbf{q}}) + \boldsymbol{\Xi}_{\mathbf{G}}(\mathbf{q}, \dot{\mathbf{q}})\ddot{\mathbf{q}})$. ■

B.6 Proof of Theorem 4

Theorem 4. *Suppose \mathcal{C} is related to K leaf-node task spaces by maps $\{\psi_i : \mathcal{C} \rightarrow \mathcal{T}_i\}_{i=1}^K$ and the i th task space \mathcal{T}_i has an affine connection $G_i \nabla$ on $T\mathcal{T}_i$, as defined in Theorem 3, and a covector function F_i defined by some potential and damping as described above. Let ${}^G\nabla = \sum_{i=1}^K T\psi_i^* G_i \nabla$ be the pullback connection, $G = \sum_{i=1}^K T\psi_i^* G_i$ be the pullback metric, and $F = \sum_{i=1}^K T\psi_i^* F_i$ be the pullback covector, where $T\psi_i^* : T^*T\mathcal{T}_i \rightarrow T^*T\mathcal{C}$. Then ${}^G\nabla$ is compatible with G , and $\text{pr}_3({}^G\nabla_{\ddot{q}}\ddot{q}) = (\text{pr}_3 \circ G^\sharp \circ F)(s)$ can be written as $\ddot{\mathbf{q}} + \mathbf{G}(\mathbf{q}, \dot{\mathbf{q}})^{-1} (\boldsymbol{\eta}_{\mathbf{G};\mathcal{S}}(\mathbf{q}, \dot{\mathbf{q}}) + \boldsymbol{\Xi}_{\mathbf{G}}(\mathbf{q}, \dot{\mathbf{q}})\ddot{\mathbf{q}}) = -\mathbf{G}(\mathbf{q}, \dot{\mathbf{q}})^{-1} (\nabla_{\mathbf{q}}\Phi(\mathbf{q}) + \mathbf{B}(\mathbf{q}, \dot{\mathbf{q}})\dot{\mathbf{q}})$. In particular, if G is velocity-independent, then ${}^G\nabla = {}^G\nabla$.*

Proof of Theorem 4. Let $\mathcal{T} = \mathcal{T}_1 \times \dots \times \mathcal{T}_K$ and \tilde{G} be the induced metric on $T\mathcal{T}$ by $\{G_i\}_{i=1}^K$. In addition, let $\psi : \mathcal{C} \rightarrow \mathcal{T}$ be the equivalent expression of $\{\psi_i\}$. Again we focus on the tangent bundle not the base manifold. Recall the definition of a pullback connection¹⁰ $T\psi^* \tilde{G} \nabla$ is

$$T\psi_*(T\psi^* \tilde{G} \nabla_X Y) = \text{pr}_{T\psi_*}^{\tilde{G}} \left(\tilde{G} \nabla_{T\psi_* X} T\psi_* Y \right) \quad (10)$$

for all sections X and Y on $T\mathcal{T}\mathcal{C}$, where $\text{pr}_{T\psi_*}^{\tilde{G}}$ is the projection onto the distribution spanned by $T\psi_*$ with respect to \tilde{G} , i.e. $\tilde{G}(T\psi_* X, \text{pr}_{T\psi_*}^{\tilde{G}}(Z)) = \tilde{G}(T\psi_* X, Z)$ for all $X \in T\mathcal{T}\mathcal{C}$ and $Z \in T\mathcal{T}\mathcal{T}$. Note by the construction of the product manifold \mathcal{T} , $T\psi^* \tilde{G} \nabla = \sum_{i=1}^K T\psi_i^* G_i \nabla$.

Compatibility We show that $T\psi^* \tilde{G} \nabla$ is compatible with the pullback metric G . Let X, Y, Z be arbitrary sections on $T\mathcal{T}\mathcal{C}$ and recall the definition of the pullback metric

$$G(X, Y) = T\psi^* \tilde{G}(X, Y) = \tilde{G}(T\psi_* X, T\psi_* Y)$$

¹⁰ We note the distinction between $\psi^* : T^*\mathcal{T} \rightarrow T^*\mathcal{C}$ and $T\psi^* : T^*T\mathcal{T} \rightarrow T^*T\mathcal{C}$.

To show that $T\psi^*\tilde{G}\nabla$ is compatible, we derive an expression of $G(T\psi^*\tilde{G}\nabla_Z X, Y)$:

$$\begin{aligned}
G(T\psi^*\tilde{G}\nabla_Z X, Y) &= T\psi^*\tilde{G}(T\psi^*\tilde{G}\nabla_Z X, Y) \\
&= \tilde{G}(T\psi_*(T\psi^*\tilde{G}\nabla_Z X), T\psi_*Y) \\
&= \tilde{G}\left(\text{pr}_{T\psi_*}^{\tilde{G}}\left(\tilde{G}\nabla_{T\psi_*Z}T\psi_*X\right), T\psi_*Y\right) \\
&= \tilde{G}\left(\tilde{G}\nabla_{T\psi_*Z}T\psi_*X, T\psi_*Y\right)
\end{aligned}$$

where we use (10) and the definition of projection. Using the above equation, we can see the compatibility easily:

$$\begin{aligned}
&G(T\psi^*\tilde{G}\nabla_Z X, Y) + G(X, T\psi^*\tilde{G}\nabla_Z Y) \\
&= \tilde{G}\left(\tilde{G}\nabla_{T\psi_*Z}T\psi_*X, T\psi_*Y\right) + \tilde{G}\left(T\psi_*X, \tilde{G}\nabla_{T\psi_*Z}T\psi_*Y\right) \\
&= \tilde{G}\nabla_{T\psi_*Z}\tilde{G}(T\psi_*X, T\psi_*Y) \\
&= \psi^*G\nabla_Z\tilde{G}(T\psi_*X, T\psi_*Y) \\
&= \psi^*G\nabla_ZG(X, Y)
\end{aligned}$$

Coordinate expression The coordinate expression of the pullback metric can be derived by its definition in (10), and the expression for the pullback covector is standard. For the pullback connection, similar to the proof of Theorem 3, we can show that $\text{pr}_3^{(G}\bar{\nabla}_{\dot{q}}\ddot{q})}$ can be written as $\ddot{\mathbf{q}} + \mathbf{G}(\mathbf{q}, \dot{\mathbf{q}})^{-1}(\boldsymbol{\eta}_{\mathbf{G};S}(\mathbf{q}, \dot{\mathbf{q}}) + \boldsymbol{\Xi}_{\mathbf{G}}(\mathbf{q}, \dot{\mathbf{q}})\ddot{\mathbf{q}})$. In other words, the structured GDS equations are the coordinate expression of the pullback connection $T\psi^*\tilde{G}\nabla$, where the structure \mathcal{S} is induced through the recursive application of `pullback` in RMPflow. Note that this is in general different from the connection of the pullback metric ${}^G\nabla$, which by Theorem 3 instead defines the unstructured GDS equation $\ddot{\mathbf{q}} + \mathbf{G}(\mathbf{q}, \dot{\mathbf{q}})^{-1}(\boldsymbol{\xi}_{\mathbf{G}}(\mathbf{q}, \dot{\mathbf{q}}) + \boldsymbol{\Xi}_{\mathbf{G}}(\mathbf{q}, \dot{\mathbf{q}})\ddot{\mathbf{q}})$.

Commutability However, in the special case when G is velocity-independent, we show that they are equivalent. That is, the pullback connection $T\psi^*\tilde{G}\nabla$ is equal to the connection of the pullback matrix ${}^G\nabla$. This property is early shown in Theorem 1, which shows that in the velocity-independent case there is no need to distinguish structures. To prove this, we first note that ${}^G\nabla$ becomes symmetric as G is velocity-independent. As it is also compatible with G , we know that ${}^G\nabla$ is the Levi-Civita connection with respect to G . (Recall G is the Riemannian metric on the tangent bundle.) On the other hand, knowing that $T\psi^*\tilde{G}\nabla$ is compatible, to show that ${}^G\nabla = T\psi^*\tilde{G}\nabla$ we only need to check if $T\psi^*\tilde{G}\nabla$ is symmetric. Without further details, we note this is implied by the proof of Theorem 1. Therefore, we have $T\psi^*\tilde{G}\nabla = {}^G\nabla$. ■

C Relationship between RMPflow and Recursive Newton-Euler Algorithms

The policy generation procedure of RMPflow is closely related to the algorithms [17] for computing forward dynamics (i.e. computing accelerations given forces) based on recursive Newton-Euler algorithm. In a summary, these algorithms compute the forward dynamics in following steps:

1. It propagates positions and velocities from the base to the end-effector.
2. It computes the Coriolis force by backward propagating the inverse dynamics of each link under the condition that the acceleration is zero.
3. It computes the (full/upper-triangular/lower-triangular) joint inertia matrix.
4. It solves a linear system of equations to obtain the joint acceleration.

In [17], they assume a recursive Newton-Euler algorithm (RNE) for inverse dynamics is given, and realize Step 1 and Step 2 above by calling the RNE subroutine. The computation of Step 3 depends on which part of the inertia matrix is computed. In particular, their Method 3 (also called the Composite-Rigid-Body Algorithm in [33, Chapter 6]) computes the upper triangle part of the inertia matrix by a backward propagation from the end-effector to the base.

RMPflow can also be used to compute forward dynamics, when we set the leaf-node GDS as the constant inertia system on the body frame of each link and we set the transformation in the RMP-tree as the change of coordinates across of robot links. This works because we show GDSs cover SMSs as a special case, and at root node the effective dynamics is the pullback GDS, which in this case is the effective robot dynamics defined by the inertia matrix of each link.

We can use this special case to compare RMPflow with the above procedure. We see that the forward pass of RMPflow is equivalent to Step 1, and the backward pass of RMPflow is equivalent of Step 2 and Step 3, and the final `resolve` operation is equivalent to Step 4.

Despite similarity, the main difference is that RMPflow computes the force and the inertia matrix in a *single* backward pass to exploit shared computations. This change is important, especially, the number of subtasks are large, e.g., in avoiding multiple obstacles. In addition, the design of RMPflow generalizes these classical computational procedures (e.g. designed only for rigid bodies, rotational/prismatic joints) to handle abstract and even non-Euclidean task spaces that have velocity-dependent metrics/inertias. This extension provides a unified framework of different algorithms and results in an expressive class of motion policies.

D Designing Reactive Motion Policies for Manipulation

In this section, we give some details on the RMPs examples discussed in Section 3.6, which are also used in our manipulation system in the full system experiments. We show that these commonly used motion policies are essentially

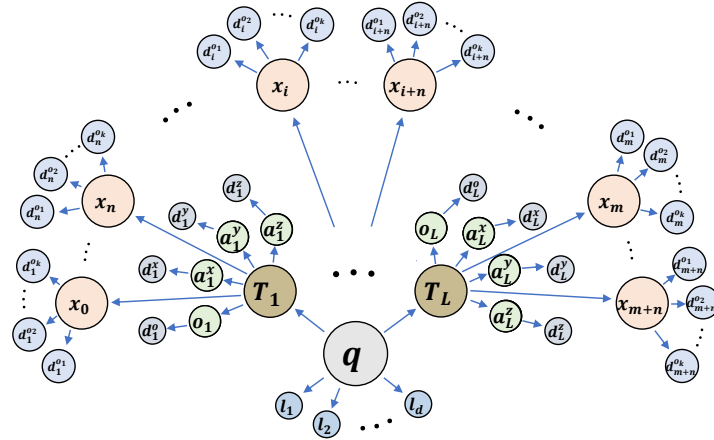


Fig. 6: This figure depicts the tree of task maps used in the experiments. See Section D.1 for details.

GDSs with respect to some metric and potential function. To convert a differential equation back to its GDS formulation, we need to address the question of integrability of a vector field. This is done by showing that a hand-designed vector field is the negative gradient of some potential function. It is useful in these cases to remember that the necessary and sufficient condition on the integrability of a smooth vector field is that its Jacobian is symmetric.

D.1 Task map and its Tree Structure

Figure 6 depicts the tree of task maps used in the full-robot experiments. The chosen structure emphasizes potential for parallelization over fully exploiting the recursive nature of the kinematic chain, treating each link frame as just one forward kinematic map step from the configuration space.¹¹ The configuration space \mathbf{q} is linked to L link frames $\mathbf{T}_1, \dots, \mathbf{T}_L$ through the robot’s forward kinematics. Each frame has 4 frame element spaces: the origin o_i and each of the axes $\mathbf{a}_i^x, \mathbf{a}_i^y, \mathbf{a}_i^z$, with corresponding distance spaces to targets $d_i^o, d_i^x, d_i^y, d_i^z$ (if they are active). Additionally, there are a number of obstacle control points \mathbf{x}_j distributed across each of the links, each with k associated distance spaces $d_j^{o1}, \dots, d_j^{ok}$, one for each obstacle o_1, \dots, o_k . Finally, for each dimension of the configuration space there’s an associated joint limit space l_1, \dots, l_d .

D.2 Example: 1D Velocity-Dependent Metrics

We start with an analysis of a simple 1-dimensional GDS with a velocity-dependent metric to provide some intuition about the curvature terms ξ and Ξ . This example will be used for constructing collision controllers later.

¹¹ We could possibly have saved some computation by defining the forward kinematic maps recursively as $(\mathbf{T}_{i+1}, \mathbf{q}_{i+1}, \dots, \mathbf{q}_d) = \psi_i(\mathbf{T}_i, \mathbf{q}_i, \dots, \mathbf{q}_d)$.

Let $z = d(\mathbf{x}) \in \mathbb{R}$ be a 1D task space; for instance, d might be a distance function with $\mathbf{x} \in \mathbb{R}^3$. Let $g(z, \dot{z})$ denote a velocity dependent metric and let $\Phi(z)$ be a potential function. This choice defines a total energy (i.e. the Lyapunov function) $V(z, \dot{z}) = \frac{1}{2}g(z, \dot{z})\dot{z}^2 + \Phi(z)$. It defines a GDS with an equation of motion under external force $f_{\text{ext}} = -\partial_z \Phi - b(z, \dot{z})\dot{z}$ as

$$\ddot{z} = \frac{1}{g + \Xi} (-\partial_z \Phi - b(z, \dot{z})\dot{z} - \xi), \quad (11)$$

where $\Xi = \frac{1}{2}\dot{z}\frac{\partial g}{\partial \dot{z}}$, ξ is the curvature term (see below), and $b(z, \dot{z}) > 0$ is the damping coefficient.

Theorem 2 provides a sufficient condition for stability. In this example, it requires $\dot{z}\frac{\partial g}{\partial \dot{z}} \geq 0$. Suppose the metric decomposes as $g(z, \dot{z}) = w(z)u(\dot{z})$. The sufficient condition of Theorem 2 becomes

$$2\Xi = \dot{z}\frac{\partial g}{\partial \dot{z}} = w(z)\dot{z}\frac{du}{d\dot{z}} \geq 0, \quad (12)$$

In other words, u needs to change (as a function of \dot{z}) in the same direction as the velocity: u either increases in the positive direction when velocity is positive and increases in the negative direction when velocity is negative; or it can be zero.

Denoting $g_z(z)$ as the corresponding function of \dot{z} that arises by fixing the value of \dot{z} , we can write the curvature terms as

$$\xi = \left(\frac{d}{dt} g_z \right) \dot{z} - \frac{d}{dz} \left(\frac{1}{2} g(z, \dot{z}) \dot{z}^2 \right) \quad (13)$$

$$= u(\dot{z}) \left(\frac{d}{dt} w(z) \right) \dot{z} - u(\dot{z}) \frac{d}{dz} \left(\frac{1}{2} w(z) \dot{z}^2 \right) \quad (14)$$

$$= u(\dot{z}) \left(\frac{dw}{dz} \dot{z}^2 - \frac{1}{2} \frac{dw}{dz} \dot{z}^2 \right) \quad (15)$$

$$= \frac{1}{2} u \frac{dw}{dz} \dot{z}^2. \quad (16)$$

Therefore $-\xi = -\frac{1}{2}u\frac{dw}{dz}\dot{z}^2$ is a force that always points along decreasing w .

D.3 Collision Avoidance Controllers

Here we derive a class of 1D collision controllers defined on the distance space, and show that the curvature terms in the pullback to $\mathbf{x} \in \mathbb{R}^3$ define nontrivial curving terms that induce the types of orbits that we see in Figure 3.

Let $s = d(\mathbf{x})$ for $\mathbf{x} \in \mathbb{R}^3$ denote a distance function $d : \mathbb{R}^3 \rightarrow \mathbb{R}_+$. Let $g(s, \dot{s}) = w(s)u(\dot{s})$ denote a 1D separable velocity-dependent metric. $w(s)$ is defined as a non-increasing function in s , i.e. and $s_1 \leq s_2 \Rightarrow w(s_1) \geq w(s_2)$ and hence $\frac{dw}{ds} \leq 0$ for all $s \in \mathbb{R}_+$. Typically, $w(s) = 0$ for $s > r_w$ for some nominal radius of action $r_w > 0$. For instance, we might choose

$$w(s) = \frac{(r_w - s)_+^2}{s}, \quad (17)$$

where $(v)_+ = \max\{0, v\}$. For this function, $w(r_w) = 0$ and differentiating it shows that $\frac{dw}{ds} = 1 - \frac{r_w^2}{s^2} < 0$ for $s \in (0, r_w)$ and 0 for $s \geq r_w$. The equality only holds at $s = r_w$ (i.e. when w is tangent to the s axis at $s = r_w$). Its Hessian can be shown as $\frac{d^2w}{ds^2} = \frac{2r_w^2}{s^3} > 0$ for $s > 0$ (i.e. positive definite). Likewise we choose

$$u(\dot{s}) = \begin{cases} 1 - \exp\left(-\frac{\dot{s}^2}{2\sigma^2}\right), & \text{for } \dot{s} < 0 \\ 0, & \text{otherwise} \end{cases} \quad (18)$$

It is straightforward to show that this choice satisfies the condition in (12), and $u(\dot{s}) \in [0, 1)$ with a smooth transition to 0 for $\dot{s} \geq 0$.

Suppose $\Phi : \mathbb{R}_+ \rightarrow \mathbb{R}$ is a potential function that is continuously differentiable. As discussed, the GDS would have an equation of motion in the form

$$\ddot{s}^d = -\frac{1}{m} \frac{d\Phi_0}{ds} - \frac{1}{m} \xi$$

where we recall $m(s, \dot{s}) = g(s, \dot{s}) + \Xi(s, \dot{s})$ and Ξ and ξ are the curvature terms. Particularly, for our chosen product metric $g(s, \dot{s}) = w(s)u(\dot{s})$, we can write $\xi(s, \dot{s}) = \frac{1}{2}u(\dot{s})\frac{dw}{ds}\dot{s}^2$, $\Xi(s, \dot{s}) = \frac{1}{2}w(s)\dot{s}\frac{du}{d\dot{s}}$ (cf. the previous section), and

$$\begin{aligned} m(s, \dot{s}) &= w(s)u(\dot{s}) + \frac{1}{2}w(s)\dot{s}\frac{du}{d\dot{s}} \\ &= w(s) \left(u(\dot{s}) + \frac{1}{2}\dot{s}\frac{du}{d\dot{s}} \right) =: w(s)\delta(s, \dot{s}) \end{aligned}$$

which also has a product structure.

This factorization shows that the equation of motion can also be written as

$$\begin{aligned} \ddot{s}^d &= -\frac{1}{\delta} \left(\frac{1}{w} \frac{d\Phi}{ds} \right) - \frac{1}{m} \xi \\ &= -\frac{1}{\delta} \left(\frac{d\tilde{\Phi}}{ds} \right) - \frac{1}{w} \tilde{\xi} \end{aligned}$$

for some function $\tilde{\Phi}$ and $\tilde{\xi} = \frac{1}{2}\frac{dw}{ds}\dot{s}^2$ is the curvature term if w is considered as a (velocity-independent) metric. This identification is possible because $\frac{1}{w}\frac{d\Phi}{ds}$ is continuous and s is one-dimensional. Conversely, we can start with designing a continuous vector field $\frac{d\tilde{\Phi}}{ds}$, i.e. choosing a vector field $\frac{d\tilde{\Phi}}{ds}$ such that $\ddot{s}^d = -\frac{1}{\delta} \left(\frac{d\tilde{\Phi}}{ds} \right) - \frac{1}{m} \xi$ has the desired behavior. And the above identification shows that this equation of motion is a GDS.

To represent the above equation as an RMP, which is useful if we choose to design behavior by directly defining $\frac{d\tilde{\Phi}}{ds}$, we can write it in the natural form as

$$\left[-w \frac{d\tilde{\Phi}}{ds} - \xi, m \right]^{\mathbb{R}_+}. \quad (19)$$

Note that the curvature term ξ behaves as a nonlinear damping term, slowing the system (from the perspective of the configuration space) as it approaches obstacles and vanishing when moving away from obstacles. Consequently, it biases the system toward curving along isocontours of the distance field. See Fig. 3 for a demonstration of these terms in isolation and in coordination with an obstacle repulsion potential.

D.4 Attractors

We detail a couple of attractor options here, including two metrics that we have used in practice. We sometimes find the more complex of these metrics works better on collision avoidance systems, since it expresses a desire for precision near the target while allowing orthogonal compliance further away giving some freedom for obstacle avoidance.

Notation Let \mathbf{x} be the coordinate of the task space (e.g. the coordinate of the task space). We denote the inertia matrix as $\mathbf{M}(\mathbf{x})$, the forcing potential function as $\Phi(\mathbf{x})$, and the damping matrix as $\mathbf{B}(\mathbf{x}, \dot{\mathbf{x}})$. In this section, for designing attractors, we will focus on the special case where $\mathbf{M}(\mathbf{x}) = \mathbf{G}(\mathbf{x})$.

Acceleration-based attractors and GDSs In many cases, it is straightforward to design a task space behavior in isolation in terms of desired accelerations (either by hand or through planning) [16]. But for stability guarantees we want these systems to be GDSs. Specifically, suppose we have a motion policy given as $\mathbf{f}(\mathbf{x}, \dot{\mathbf{x}})$. Define $\ddot{\mathbf{x}}^d = \mathbf{f}(\mathbf{x}, \dot{\mathbf{x}})$ as a shorthand (i.e. the desired acceleration). We want to show that it can be written as

$$\ddot{\mathbf{x}}^d = -\mathbf{M}(\mathbf{x})^{-1} \left(\nabla_{\mathbf{x}} \Phi(\mathbf{x}) + \boldsymbol{\xi}_{\mathbf{M}}(\mathbf{x}, \dot{\mathbf{x}}) + \mathbf{B}(\mathbf{x}, \dot{\mathbf{x}}) \dot{\mathbf{x}} \right) \quad (20)$$

for some \mathbf{M} , \mathbf{B} , and Φ , where $\boldsymbol{\xi}_{\mathbf{M}}$ is the associated curvature term of \mathbf{M} . We can view the above decomposition as three parts:

1. The desired acceleration generated by the potential: $-\mathbf{M}(\mathbf{x})^{-1} \nabla \Phi(\mathbf{x})$
2. The damping acceleration for stability: $-\mathbf{M}(\mathbf{x})^{-1} \mathbf{B}(\mathbf{x}, \dot{\mathbf{x}}) \dot{\mathbf{x}}$
3. The curvature acceleration for consistent behaviors: $-\mathbf{M}(\mathbf{x})^{-1} \boldsymbol{\xi}_{\mathbf{M}}(\mathbf{x}, \dot{\mathbf{x}})$

To bridge the connection between the GDS formulation in (20) and common motion policies given directly by \mathbf{f} , we consider particularly motion policy candidates that can be written in terms of

$$\ddot{\mathbf{x}}^d = -\nabla_{\mathbf{x}} \tilde{\Phi}(\mathbf{x}) - \tilde{\mathbf{B}}(\mathbf{x}, \dot{\mathbf{x}}) \dot{\mathbf{x}} - \mathbf{M}(\mathbf{x})^{-1} \boldsymbol{\xi}_{\mathbf{M}}(\mathbf{x}, \dot{\mathbf{x}}) \quad (21)$$

where $\tilde{\Phi}$ is another potential function and $\tilde{\mathbf{B}}(\mathbf{x}, \dot{\mathbf{x}})$ is another damping matrix. We show that it is possible to design $\tilde{\Phi}$ and $\tilde{\mathbf{B}}$ directly, and then choose some proper inertia matrix $\mathbf{M}(\mathbf{x})$ such that (21) can be written as the GDS (20) for some Φ and \mathbf{B} . That is, we show it possible to choose \mathbf{M} such that

$$\nabla_{\mathbf{x}} \Phi(\mathbf{x}) = \mathbf{M}(\mathbf{x}) \nabla_{\mathbf{x}} \tilde{\Phi}(\mathbf{x}) \quad \text{and} \quad \mathbf{B}(\mathbf{x}, \dot{\mathbf{x}}) = \mathbf{M}(\mathbf{x}) \tilde{\mathbf{B}}(\mathbf{x}, \dot{\mathbf{x}})$$

and Φ is a potential function and \mathbf{B} is positive definite (without the need to derive them in closed form). Moreover, we show that this strategy allows us to model some common acceleration-based attractors.

Motion policy candidates As a motivating example of (21), we consider the attractor proposed in [16]. Let h_V^α define a *soft-normalization* function

$$\theta_\alpha(\mathbf{v}) = \mathbf{v}/h_V^\alpha(\|\mathbf{v}\|). \quad (22)$$

with $h_V^\alpha(\gamma) = \frac{1}{\alpha} \log(e^{\alpha\gamma} + e^{-\alpha\gamma}) = \gamma + \frac{1}{\alpha} \log(1 + e^{-2\alpha\gamma})$ for some $\alpha > 0$, so that $\theta_\alpha(\mathbf{v})$ approaches $\hat{\mathbf{v}} = \frac{\mathbf{v}}{\|\mathbf{v}\|}$ for larger \mathbf{v} , but approaches zero smoothly as $\mathbf{v} \rightarrow 0$. Without loss of generality, let us consider the center of attraction is at $\mathbf{x} = 0$. The attractor considered in [16] is given as

$$\ddot{\mathbf{x}}^d = \mathbf{f}_a(\mathbf{x}, \dot{\mathbf{x}}) := -\gamma_p \theta_\alpha(\mathbf{x}) - \gamma_d \dot{\mathbf{x}}, \quad (23)$$

for some $\gamma_p, \gamma_d > 0$.

Inspecting (23), we can see that it resembles the form (21) modulus the last curvature term $-\mathbf{M}(\mathbf{x})^{-1} \boldsymbol{\xi}(\mathbf{x}, \dot{\mathbf{x}})$. Indeed we can identify $\tilde{\mathbf{B}} = \gamma_d \mathbf{I}$ and we show below the first term $\gamma_p \theta_\alpha(\mathbf{x}_0 - \mathbf{x})$ is a derivative of some potential function. We do so by showing its Jacobian is symmetric. Using the notation above, we have

$$\begin{aligned} \frac{d}{d\mathbf{x}} \theta_\alpha(\mathbf{x}) &= \frac{d}{d\mathbf{x}} (h_V^\alpha(\|\mathbf{x}\|)^{-1} \mathbf{x}) \\ &= h_V^\alpha(\|\mathbf{x}\|)^{-1} \mathbf{I} + \mathbf{x} \left(-h_V^\alpha(\|\mathbf{x}\|)^{-2} \frac{dh_V^\alpha(s)}{ds} \Big|_{s=\|\mathbf{x}\|} \frac{\partial}{\partial \mathbf{x}} \|\mathbf{x}\| \right) \\ &= h_V^\alpha(\|\mathbf{x}\|)^{-1} \mathbf{I} - \left(\|\mathbf{x}\| h_V^\alpha(\|\mathbf{x}\|)^{-2} \frac{dh_V^\alpha(s)}{ds} \Big|_{s=\|\mathbf{x}\|} \right) \hat{\mathbf{x}} \hat{\mathbf{x}}^T. \end{aligned}$$

Both terms are symmetric, so the Jacobian is symmetric and this vector field is the gradient of some potential function (say $\tilde{\Phi}_a^1$), although we do not attempt to derive the potential function in closed form here.

In some cases, it is potentially more convenient to start designing (21) with a known potential function such as

$$\begin{aligned} \tilde{\Phi}_a^2(\mathbf{x}) &= \frac{1}{\eta} \log \left(e^{\eta\|\mathbf{x}\|} + e^{-\eta\|\mathbf{x}\|} \right) \\ &= \|\mathbf{x}\| + \frac{1}{\eta} \log \left(1 + e^{-2\eta\|\mathbf{x}\|} \right) \end{aligned} \quad (24)$$

so the potential energy can be measured, where $\eta > 0$. This is a η -scaled softmax (η defines the effective smoothing radius at the origin) over $\|\mathbf{x}\|$ and $-\|\mathbf{x}\|$, and the second expression is a numerically robust version since $\|\mathbf{x}\| \geq 0$. Its negative

gradient is

$$\begin{aligned}\nabla_{\mathbf{x}}\tilde{\Phi}^2(\mathbf{x}) &= \frac{1}{\alpha e^{\alpha\|\mathbf{x}\|} + e^{-\alpha\|\mathbf{x}\|}} \left(\alpha e^{\alpha\|\mathbf{x}\|} \hat{\mathbf{x}} - \alpha e^{-\alpha\|\mathbf{x}\|} \hat{\mathbf{x}} \right) \\ &= \left(\frac{e^{\alpha\|\mathbf{x}\|} - e^{-\alpha\|\mathbf{x}\|}}{e^{\alpha\|\mathbf{x}\|} + e^{-\alpha\|\mathbf{x}\|}} \right) \hat{\mathbf{x}} \\ &= \left(\frac{1 - e^{-2\alpha\|\mathbf{x}\|}}{1 + e^{-2\alpha\|\mathbf{x}\|}} \right) \hat{\mathbf{x}} = s_{\alpha}(\|\mathbf{x}\|) \hat{\mathbf{x}},\end{aligned}\tag{25}$$

where $s_{\alpha}(0) = 0$ and $s_{\alpha}(r) \rightarrow 1$ as $r \rightarrow \infty$. (25) again gives a numerically robust form since $\|\mathbf{x}\| \geq 0$. Below, we denote abstractly the potential as just $\tilde{\Phi}$ so we're agnostic to the choice of $\tilde{\Phi}_a^i$, $i \in \{1, 2\}$.

Metric options Suppose we have chosen some potential $\tilde{\Phi}$ and some damping $\tilde{\mathbf{B}}$. We next consider admissible metric/inertia matrices such that (21) can be written as (20). We first note that $\mathbf{M} = \mathbf{I}$ is an admissible choice (i.e. we recover $\Phi(\mathbf{x}) = \tilde{\Phi}$ and $\mathbf{B} = \tilde{\mathbf{B}}$, provided $\tilde{\mathbf{B}}$ is positive definite). But this choice is not ideal when we wish to combine multiple motion policies, because we recall that the design of \mathbf{M} designates the importance of each motion policy. Therefore, we would not want to restrict ourselves to the trivial choice $\mathbf{M} = \mathbf{I}$.

Here we present a family of metric matrices that are non-trivial and meaningful in practice, and yet is *compatible* with the motion policy (21). Let us first define some useful functions to simplify the writing later on. Let $\alpha(\mathbf{x}) = \exp(-\frac{\|\mathbf{x}\|^2}{2\sigma_{\alpha}^2})$ and $\gamma(\mathbf{x}) = \exp(-\frac{\|\mathbf{x}\|^2}{2\sigma_{\gamma}^2})$ for some $\sigma_{\alpha}, \sigma_{\gamma} \in \mathbb{R}$. We define a weight function $w(\mathbf{x}) = \gamma(\mathbf{x})w_u + (1 - \gamma(\mathbf{x}))w_l$, for $0 \leq w_l \leq w_u < \infty$. Equivalently, it can be written as $w(\mathbf{x}) = \hat{w}\gamma(\mathbf{x}) + w_l$ with $\hat{w} := w_u - w_l$. Below we will need $\nabla_{\mathbf{x}} \log w(\mathbf{x})$, so we derive it here. Noting $w = \hat{w}\gamma + w_l$, we get

$$\nabla_{\mathbf{x}} \log w(\mathbf{x}) = \frac{\nabla_{\mathbf{x}}(\hat{w}\gamma + w_l)}{w(\mathbf{x})} = \frac{\hat{w}}{w} \exp\left(-\frac{\|\mathbf{x}\|^2}{2\sigma_{\gamma}^2}\right) \left(-\frac{1}{\sigma_{\gamma}^2} \mathbf{x}\right) = -\frac{\gamma \hat{w}}{\sigma_{\gamma}^2 w} \mathbf{x}.$$

We define two alternative metrics. The first metric trades off stretching the space in the direction toward the target when the robot is away from the goal, and becoming increasingly Euclidean when the robot is close to the goal:

$$\mathbf{M}_{\text{stretch}} = w(\mathbf{x}) \left((1 - \alpha(\mathbf{x})) \nabla_{\mathbf{x}} \tilde{\Phi} \nabla_{\mathbf{x}} \tilde{\Phi}^{\top} + (\alpha(\mathbf{x}) + \epsilon) \mathbf{I} \right),\tag{26}$$

where $\epsilon > 0$ induces a baseline Euclidean metric used far from the target to fill out the metric's eigen-spectrum, and $\tilde{\Phi}$ is the potential in (21). The second metric matrix is simply

$$\mathbf{M}_{\text{uni}} = w(\mathbf{x}) \mathbf{I}.\tag{27}$$

We refer to these both generically as \mathbf{M} below. Note again that we use \mathbf{M} here rather than \mathbf{G} since these metrics are velocity independent so that the inertia matrix \mathbf{M} and the metric (typically denoted as \mathbf{G}) are the same.

Compatibility between metrics and potentials We show the two metrics $\mathbf{M}_{\text{stretch}}$ and \mathbf{M}_{uni} above are compatible with $\tilde{\Phi}_a^i$, $i \in \{1, 2\}$. For simplicity, let us denote them just as \mathbf{M} and $\tilde{\Phi}$. We will show that there exists a potential Φ such that $\nabla_{\mathbf{x}}\Phi = \mathbf{M}\nabla_{\mathbf{x}}\tilde{\Phi}$. In fact, our result applies to potentials more general than $\tilde{\Phi}_a^i$ for $i \in \{1, 2\}$. It applies to all potentials $\tilde{\Phi}(\mathbf{x})$ such that $\nabla_{\mathbf{x}}\tilde{\Phi}(\mathbf{x}) = \kappa(\|\mathbf{x}\|)\hat{\mathbf{x}}$ for some function $\kappa : \mathbb{R} \rightarrow \mathbb{R}$, which includes $\tilde{\Phi}_a^i$ for $i \in \{1, 2\}$ as special cases.

We prove the existence by analyzing the Jacobian of $\mathbf{M}\nabla_{\mathbf{x}}\tilde{\Phi}$ and showing that it is symmetric. We first note that a result of radial symmetry.

Lemma 6. *Let $\nabla_{\mathbf{x}}\tilde{\Phi}(\mathbf{x}) = \kappa(\|\mathbf{x}\|)\hat{\mathbf{x}}$ for some $\kappa : \mathbb{R} \rightarrow \mathbb{R}$ operating on the distance to the origin, and let f be a differentiable function. Then the Jacobian matrix*

$$\frac{\partial}{\partial \mathbf{x}}(f\nabla_{\mathbf{x}}\tilde{\Phi}) = f(\mathbf{x})\nabla_{\mathbf{x}}^2\tilde{\Phi} + \kappa(\mathbf{x})f'(\|\mathbf{x}\|)\hat{\mathbf{x}}\hat{\mathbf{x}}^\top \quad (28)$$

is symmetric.

Proof. We first note that $\nabla f(\|\mathbf{x}\|) = f'(\|\mathbf{x}\|)\hat{\mathbf{x}}$ for all differentiable f . Then the results follow directly as the derivation below

$$\begin{aligned} \frac{\partial}{\partial \mathbf{x}}(f\nabla_{\mathbf{x}}\tilde{\Phi}) &= f(\mathbf{x})\nabla_{\mathbf{x}}^2\tilde{\Phi} + \nabla\tilde{\Phi}\nabla f^\top \\ &= f(\mathbf{x})\nabla_{\mathbf{x}}^2\tilde{\Phi} + \gamma(\mathbf{x})f'(\|\mathbf{x}\|)\hat{\mathbf{x}}\hat{\mathbf{x}}^\top \end{aligned} \quad (29)$$

because the Hessian $\nabla^2\tilde{\Phi}$ is symmetric. ■

Given Lemma 6, showing symmetry of the Jacobian of $\mathbf{M}\nabla_{\mathbf{x}}\tilde{\Phi}$ is straightforward, because both $\tilde{\Phi}$ considered satisfy $\nabla\tilde{\Phi} = \kappa(\|\mathbf{x}\|)\hat{\mathbf{x}}$ for some κ . First, we consider \mathbf{M}_{uni} . We can write $\mathbf{M}_{\text{uni}}\nabla\tilde{\Phi} = w(\mathbf{x})\nabla\tilde{\Phi}$ and $w(\mathbf{x}) = \tilde{w}(\|\mathbf{x}\|)$ with $\tilde{w}(s) = \hat{w}\exp(-\frac{s^2}{2\sigma_\gamma}) + w_l$, so its Jacobian is symmetric. Similarly,

$$\begin{aligned} \mathbf{M}_{\text{stretch}}\nabla\tilde{\Phi} &= w(\mathbf{x})\left((1 - \alpha(\mathbf{x}))\nabla_{\mathbf{x}}\tilde{\Phi}\nabla_{\mathbf{x}}\tilde{\Phi}^\top + \alpha(\mathbf{x})\right)\nabla_{\mathbf{x}}\tilde{\Phi} \\ &= w(\mathbf{x})\left((1 - \alpha(\mathbf{x}))\|\nabla_{\mathbf{x}}\tilde{\Phi}\|^2\nabla_{\mathbf{x}}\tilde{\Phi} + \alpha(\mathbf{x})\nabla_{\mathbf{x}}\tilde{\Phi}\right) \\ &= \tilde{w}(\|\mathbf{x}\|)h(\|\mathbf{x}\|)\nabla_{\mathbf{x}}\tilde{\Phi}, \end{aligned}$$

where $h(s) = (1 - \tilde{\alpha}(s))\kappa(s)^2 + \tilde{\alpha}(s)$ with $\tilde{\alpha}(s) = \exp(-\frac{s^2}{2\sigma_\alpha})$. This expression fits in the form considered in Lemma 6 and therefore it has a symmetric Jacobian.

Compatibility between metrics and damping The condition for the damping part is relative straightforward. We simply need to choose $\tilde{\mathbf{B}}$ such that

$$\mathbf{B}(\mathbf{x}, \dot{\mathbf{x}}) = \mathbf{M}(\mathbf{x})\tilde{\mathbf{B}}(\mathbf{x}, \dot{\mathbf{x}}) \succ 0$$

A sufficient condition is to set $\tilde{\mathbf{B}}$ to share the same eigen-system as \mathbf{M} .

Effects of the curvature term We have provided conditions for compatibility between metrics, potentials, and damping. We now consider the effects of the curvature acceleration $-\mathbf{M}(\mathbf{x})^{-1}\boldsymbol{\xi}_{\mathbf{M}}(\mathbf{x}, \dot{\mathbf{x}})$

$$\ddot{\mathbf{x}}^d = -\nabla_{\mathbf{x}}\tilde{\Phi}(\mathbf{x}) - \tilde{\mathbf{B}}(\mathbf{x}, \dot{\mathbf{x}})\dot{\mathbf{x}} - \mathbf{M}(\mathbf{x})^{-1}\boldsymbol{\xi}_{\mathbf{M}}(\mathbf{x}, \dot{\mathbf{x}}) \quad (21)$$

due to our non-trivial choice of metric matrix.

For $\mathbf{M}_{\text{uni}} = w(\mathbf{x})\mathbf{I}$, this becomes

$$\begin{aligned} \boldsymbol{\xi}_{\mathbf{M}} &= \frac{dw}{dt}\dot{\mathbf{x}} - \frac{1}{2}\nabla_{\mathbf{x}}w\|\dot{\mathbf{x}}\|^2 \\ &= (\dot{\mathbf{x}}^\top\nabla_{\mathbf{x}}w)\dot{\mathbf{x}} - \frac{1}{2}\nabla_{\mathbf{x}}w\|\dot{\mathbf{x}}\|^2 \\ &= \left((\dot{\mathbf{x}}\dot{\mathbf{x}}^\top) - \frac{1}{2}\|\dot{\mathbf{x}}\|^2 \right) \nabla_{\mathbf{x}}w \\ &= -\frac{1}{2}\|\dot{\mathbf{x}}\|^2 \left(\mathbf{I} - 2\hat{\mathbf{x}}\hat{\mathbf{x}}^\top \right) \nabla_{\mathbf{x}}w \end{aligned}$$

where $\hat{\mathbf{x}} = \frac{\dot{\mathbf{x}}}{\|\dot{\mathbf{x}}\|}$. That gives

$$\begin{aligned} -\mathbf{M}_{\text{uni}}^{-1}\boldsymbol{\xi}_{\mathbf{M}} &= \frac{1}{2}\|\dot{\mathbf{x}}\|^2 \left(\mathbf{I} - 2\hat{\mathbf{x}}\hat{\mathbf{x}}^\top \right) \frac{\nabla w}{w} \\ &= \frac{1}{2}\|\dot{\mathbf{x}}\|^2 H_{\hat{\mathbf{x}}}^r[\nabla \log w], \end{aligned}$$

where $H_{\hat{\mathbf{v}}}^r[\mathbf{y}] = (\mathbf{I} - 2\hat{\mathbf{v}}\hat{\mathbf{v}}^\top)\mathbf{y}$ is the Householder reflection of \mathbf{y} across the plane normal to $\hat{\mathbf{v}}$. In this case, it acts to align the system toward the goal and provides a bit of drag.

The derivatives of $\mathbf{M}_{\text{stretch}}$ are similar but more complex. We recommend a combination of finite-differencing and automatic differentiation to systematize the calculations.

Revisiting the attractor in [16] Let us revisit our motivating example

$$\ddot{\mathbf{x}}^d = \mathbf{f}_a(\mathbf{x}, \dot{\mathbf{x}}) := -\gamma_p\theta_\alpha(\mathbf{x}) - \gamma_d\dot{\mathbf{x}}, \quad (23)$$

From using the results above, we see that (23) fits in the form in (21) but missing the curvature term $-\mathbf{M}^{-1}\boldsymbol{\xi}_{\mathbf{M}}$. As we show in Section 5.1, the curvature term provides correction for consistent behaviors and stability, which suggests that the original motion policy in [16] could lose stability in general (e.g. when the velocity is high). Nevertheless, from the above analysis, we show that if we add the curvature correction back, i.e.,

$$\ddot{\mathbf{x}} = \mathbf{f}_a(\mathbf{x}, \dot{\mathbf{x}}) - \mathbf{M}^{-1}\boldsymbol{\xi}_{\mathbf{M}}$$

then the system is provably stable.

D.5 Joint Limits

We adopt a similar approach to handling joint limits as [16], but here we modify the velocity dependent components of the metric to match our theoretical requirements for stability and fully derive the curvature terms introduced by the nonlinearities and velocity dependence. We emphasize that, due to the invariance of RMPs to reparameterization that results from our complete handling of curvature terms, the behavior of the joint limit RMPs and the way in which they interact with the rest of the system are independent of the specific implementation. That said, we derive an analogous result here to the one presented in [16] to show that these joint limit RMPs effectively scale the columns of each task space's Jacobian matrix to smoothly regulate their degrees of freedom as a function of joint limit proximity. In implementation, these RMPs can be treated as any other RMP.

Integrating RMPs with joint limits We first define a class of joint limit metrics that can be used in joint limit RMPs. We show, given a joint limit RMP, the RMP algebra defined in Section 3.4 can be seen as producing the same Jacobian modification as described in [16]. We present the result more generally here as a lemma. Note that as diagonal entries of \mathbf{A} approach infinity, entries of \mathbf{D} approach zero and the corresponding column of $\tilde{\mathbf{J}}$ vanishes.

Lemma 7 (Effect of diagonal RMPs). *Let $\{(\ddot{\mathbf{x}}_i^d, \mathbf{M}_i)^{\mathcal{T}_i}\}_{i=1}^n$ be a collection of RMPs defined on task spaces \mathcal{T}_i . Let $\tilde{\ddot{\mathbf{x}}}_i^d = \ddot{\mathbf{x}}_i^d - \mathbf{J}_i \dot{\mathbf{q}}$ and let*

$$[\mathbf{M}\ddot{\mathbf{q}}^d, \mathbf{M}]^{\mathcal{C}} = \left[\sum_i \mathbf{J}_i^T \mathbf{M}_i \tilde{\ddot{\mathbf{x}}}_i^d, \sum_i \mathbf{J}_i^T \mathbf{M}_i \mathbf{J}_i \right]^{\mathcal{C}} \quad (30)$$

denote their normal form pullback and combination to space \mathcal{C} through task maps $\psi_i : \mathcal{C} \rightarrow \mathcal{T}_i$ with Jacobians $\mathbf{J}_i = \frac{\partial \psi_i}{\partial \mathbf{q}}$. Let $[\mathbf{A}\ddot{\mathbf{q}}_l^d, \mathbf{A}]^{\mathcal{C}}$ denote an RMP with diagonal¹² a velocity-dependent metric $\mathbf{A}(\mathbf{q}, \dot{\mathbf{q}}) = \lambda \mathbf{D}(\mathbf{q}, \dot{\mathbf{q}})^{-2}$, where $\lambda > 0$. Then $[\mathbf{M}\ddot{\mathbf{q}}^d, \mathbf{M}]^{\mathcal{C}} + [\mathbf{A}\ddot{\mathbf{q}}_l^d, \mathbf{A}]^{\mathcal{C}}$ has metric $\tilde{\mathbf{M}} = \mathbf{D}^{-1} \left(\sum_i \tilde{\mathbf{J}}^T \mathbf{M}_i \tilde{\mathbf{J}} + \lambda \mathbf{I} \right) \mathbf{D}^{-1}$ and motion policy

$$\ddot{\mathbf{q}}_c^d = \mathbf{D} \left(\sum_i \tilde{\mathbf{J}}^T \mathbf{M}_i \tilde{\mathbf{J}} + \lambda \mathbf{I} \right)^\dagger \left(\sum_i \tilde{\mathbf{J}}^T \mathbf{M}_i \tilde{\ddot{\mathbf{x}}}_i^d + \lambda \mathbf{D}^{-1} \ddot{\mathbf{q}}_l^d \right) \quad (31)$$

$$= \mathbf{D} \left[\arg \min_{\ddot{\mathbf{q}}} \left(\frac{1}{2} \sum_i \|\tilde{\ddot{\mathbf{x}}}_i^d - \tilde{\mathbf{J}}_i \ddot{\mathbf{q}}\|_{\mathbf{M}_i}^2 + \frac{\lambda}{2} \|\ddot{\mathbf{q}}_l^d - \ddot{\mathbf{q}}\|^2 \right) \right], \quad (32)$$

with $\tilde{\mathbf{J}} = \mathbf{J}\mathbf{D}$ and $\tilde{\ddot{\mathbf{q}}}_l^d = \mathbf{D}^{-1} \ddot{\mathbf{q}}_l^d$.

¹² We choose this form for the diagonal dependent metric (without loss of generality since it's positive definite), to be convenient notationally below.

Proof. Writing out the sum we get

$$\begin{aligned} & [\mathbf{M}\ddot{\mathbf{q}}^d, \mathbf{M}]^C + [\mathbf{A}\ddot{\mathbf{q}}_l^d, \mathbf{A}]^C \\ &= \left[\sum_i \mathbf{J}_i^T \mathbf{M}_i \ddot{\mathbf{x}}_i^d + \lambda \mathbf{D}^{-2} \ddot{\mathbf{q}}_l^d, \sum_i \mathbf{J}_i^T \mathbf{M}_i \mathbf{J}_i + \lambda \mathbf{D}^{-2} \right]^C. \\ &= \left[\mathbf{D}^{-1} \left(\sum_i \tilde{\mathbf{J}}_i^T \mathbf{M}_i \ddot{\mathbf{x}}_i^d + \lambda \mathbf{D}^{-1} \ddot{\mathbf{q}}_l^d \right), \mathbf{D}^{-1} \left(\sum_i \tilde{\mathbf{J}}_i^T \mathbf{M}_i \tilde{\mathbf{J}}_i + \lambda \mathbf{I} \right) \mathbf{D}^{-1} \right]^C. \end{aligned}$$

This gives the expression for the metric, and the motion policy can be obtained by `resolve`:

$$\begin{aligned} \tilde{\mathbf{q}}_d &= \mathbf{D} \left(\sum_i \tilde{\mathbf{J}}_i^T \mathbf{M}_i \tilde{\mathbf{J}}_i + \lambda \mathbf{I} \right)^\dagger \left(\sum_i \tilde{\mathbf{J}}_i^T \mathbf{M}_i \ddot{\mathbf{x}}_i^d + \lambda \mathbf{D}^{-1} \ddot{\mathbf{q}}_l^d \right) \\ &= \mathbf{D} \text{ resolve} \left(\left[\sum_i \tilde{\mathbf{J}}_i^T \mathbf{M}_i \ddot{\mathbf{x}}_i^d + \lambda \mathbf{D}^{-1} \ddot{\mathbf{q}}_l^d, \sum_i \tilde{\mathbf{J}}_i^T \mathbf{M}_i \tilde{\mathbf{J}}_i + \lambda \mathbf{I} \right]^C \right), \end{aligned}$$

which is equivalent to the least squares form in (32). ■

A class of velocity-dependent joint limit metrics Here we develop a velocity dependent metric to represent joint limits. We construct it for each joint independently, denoting the joint angle by $q \in [l_l, l_u]$. Let $a(q, \dot{q})$ denote a one-dimensional velocity-dependent metric on q . We want $a \rightarrow \infty$ as q is close to the joint limit and \dot{q} heads toward the joint limit. Such a metric can be constructed using a form related to that given in [16], choosing $a = b^{-2}$ for

$$b = s(\alpha_u d + (1 - \alpha_u)1) + (1 - s)(\alpha_l d + (1 - \alpha_l)1). \quad (33)$$

with $s = \frac{q-l_l}{l_u-l_l}$, $d = 4s(1-s) = 4\left(\frac{q-l_l}{l_u-l_l}\right)\left(\frac{l_u-q}{l_u-l_l}\right)$, and velocity gates $\alpha_u = 1 - e^{-\dot{q}_+^2/(2\sigma^2)}$ and $\alpha_l = 1 - e^{-\dot{q}_-^2/(2\sigma^2)}$ for $\sigma > 0$. (Choosing $a = b^{-2}$ makes intuitive sense with regard to Lemma 7.) Since $s = \frac{q-l_l}{l_u-l_l}$ and $1-s = \frac{l_u-q}{l_u-l_l}$, s indicates whether q is close to l_u ($s \rightarrow 1$ as $q \rightarrow l_u$) while $1-s$ indicates whether it is close to l_l . Likewise, α_u indicates whether \dot{q} is moving in a positive direction and α_l indicates a negative direction. Therefore, this equation encodes a smoothed binary logic that can be read “if close to the upper limit and moving in the positive direction use d , and if close to the lower limit and moving negatively d ; in all other cases use 1.” Said another way, “if close to either limit and moving toward it, use d , otherwise use 1.” Note that $\sup d = 1$ and $d \rightarrow 0$ as $q \rightarrow \{l_l, l_u\}$, so $a = b^{-2}$ has the desired property discussed above. All that remains to be shown is that this choice of $a(q, \dot{q})$ satisfies the condition $\dot{q} \frac{\partial a}{\partial \dot{q}} \geq 0$ of Theorem 2.

Lemma 8. *The velocity-dependent metric defined by $a = b^{-2}$ with b given by (33) satisfies the sufficient condition of Theorem 2 for stability, i.e. $\frac{\partial a}{\partial \dot{q}} \dot{q} \geq 0$ for all \dot{q} .*

Proof. We start by noting

$$\frac{\partial a}{\partial \dot{q}} \dot{q} = \frac{\partial}{\partial \dot{q}} b^{-2} \dot{q} = -2b^{-3} \frac{\partial b}{\partial \dot{q}} \dot{q}. \quad (34)$$

Since $b \geq 0$ we have $\frac{\partial b}{\partial \dot{q}} \dot{q} \leq 0$ implies $\frac{\partial a}{\partial \dot{q}} \dot{q} \geq 0$. We can rearrange b to be more transparent to derivatives with respect to \dot{q} :

$$b = s(\alpha_u(d-1) + 1) + (1-s)(\alpha_l(d-1) + 1) \quad (35)$$

$$= -s(1-d)\alpha_u - (1-s)(1-d)\alpha_l + c, \quad (36)$$

$$= -\gamma_u \alpha_u - \gamma_l \alpha_l + c, \quad (37)$$

where c is independent of \dot{q} and where $\gamma_u, \gamma_l \geq 0$ and both independent of \dot{q} . Therefore, we have

$$\frac{\partial b}{\partial \dot{q}} \dot{q} = -\gamma_u \frac{\partial \alpha_u}{\partial \dot{q}} - \gamma_l \frac{\partial \alpha_l}{\partial \dot{q}}. \quad (38)$$

Since $\frac{\partial \alpha_u}{\partial \dot{q}} > 0$ for $\dot{q} > 0$ and 0 otherwise, while $\frac{\partial \alpha_l}{\partial \dot{q}} < 0$ for $\dot{q} < 0$ and 0 otherwise, Equation 38 implies $\frac{\partial b}{\partial \dot{q}} \dot{q} \leq 0$ for all \dot{q} and hence $\frac{\partial a}{\partial \dot{q}} \dot{q} \geq 0$ for all \dot{q} . ■

We note that there are other choices for joint limit metrics, including those used for obstacle avoidance. In fact, one way to create joint limit controllers would be to treat each joint limit as an obstacle. We choose to use the above limit controller due to its intuitive interpretation as a velocity-dependent modification of a controller designed in a space u with the relationship $q = (l_u - l_l)\sigma(u) + l_l$ with $\sigma(u) = 1/(1 + e^{-u})$.

Motion policies for joint-limit avoidance The differential equation $\ddot{\mathbf{q}}_l^d$ from the joint limit RMPs (see Lemma 7) encodes the curvature terms from the metric \mathbf{A} . Denoting those as $\mathbf{A}^{-1}\boldsymbol{\xi}_{\mathbf{A}}$ with $\boldsymbol{\xi}_{\mathbf{A}} = \mathbf{A}\dot{\mathbf{q}} - \frac{1}{2}\nabla_{\mathbf{q}}(\dot{\mathbf{q}}^T \mathbf{A} \dot{\mathbf{q}}) = \text{diag}(\frac{1}{2} \frac{d\mathbf{A}_{ii}}{dq_i} \dot{q}_i^2)_i$, we often choose this differential equation to be

$$\ddot{\mathbf{q}}_l^d = (\eta_p(\mathbf{q}_0 - \mathbf{q}) - \eta_d \dot{\mathbf{q}}) - \mathbf{A}^{-1}\boldsymbol{\xi}_{\mathbf{A}}, \quad (39)$$

for $\eta_p, \eta_d \geq 0$. As shown in Lemma 7, this differential equation can be viewed as a transformation $\tilde{\ddot{\mathbf{q}}}_l^d = \mathbf{D}^{-1}\ddot{\mathbf{q}}_l^d = \mathbf{A}^{\frac{1}{2}}\ddot{\mathbf{q}}_l^d$ in the final joint limit corrected expression. Since \mathbf{A} becomes large near joint limits, this transformation effectively scales up the i th dimension of $\ddot{\mathbf{q}}_l^d$ when q_i nears a joint limit and \dot{q}_i is headed toward it.

E Details of the Reaching-through-clutter Experiments

We give some details on the reaching experiments here.

E.1 Experimental method

We set up a collection of clutter-filled environments with cylindrical obstacles of varying sizes in simulation as depicted in Fig. 5, and tested the performance of RMPflow and two potential field methods on a modeled ABB YuMi robot.

Compared methods:

1. **RMPflow:** We implement RMPflow using the RMPs in Section 3.6 and detailed in Appendix D. In particular, we place collision-avoidance controllers on distance spaces $s_{ij} = d_j(\mathbf{x}_i)$, where $j = 1, \dots, m$ indexes the world obstacle o_j and $i = 1, \dots, n$ indexes the n control point along the robot’s body. Each collision-avoidance controller uses a weight function $w_o(\mathbf{x})$ that ranges from 0 when the robot is far from the obstacle to $w_o^{\max} \gg 0$ when the robot is in contact with the obstacle’s surface. Similarly, the attractor potential uses a weight function $w_a(\mathbf{x})$ that ranges from w_a^{\min} far from the target to w_a^{\max} close to the target.
2. **PF-basic:** This variant is a basic implementation of obstacle avoidance potential fields with dynamics shaping. We use the RMP framework to implement this variant by placing collision-avoidance controllers on the same body control points used in RMPflow but with isotropic metrics of the form $\mathbf{G}_o^{\text{basic}}(\mathbf{x}) = w_o^{\max} \mathbf{I}$ for each control point, with w_o^{\max} matching the value RMPflow uses. Similarly, the attractor uses the same attractor potential as RMPflow, but with a constant isotropic metric with the form $\mathbf{G}_a^{\text{basic}}(\mathbf{x}) = w_a^{\max} \mathbf{I}$.
3. **PF-nonlinear:** This variant matches PF-basic in construction, except it uses a *nonlinear* isotropic metrics of the form $\mathbf{G}_o^{\text{nl}}(\mathbf{x}_i) = w_o(\mathbf{x}) \mathbf{I}$ and $\mathbf{G}_a^{\text{nl}}(\mathbf{x}_i) = w_a(\mathbf{x}) \mathbf{I}$ for obstacle-avoidance and attraction, respectively, using weight functions matching RMPflow.

A note on curvature terms: PF-basic uses constant metrics, so has no curvature terms; PF-nonlinear has nontrivial curvature terms arising from the spatially varying metrics, but we ignore them here to match common practice from the OSC literature.

Parameter scaling of PF-basic: Isotropic metrics do not express spacial directionality toward obstacles, and that leads to an inability of the system to effectively trade off the competing controller requirements. That conflict results in more collisions and increased instability. We, therefore, compare PF-basic under these baseline metric weights (matching RMPflow) with variants that incrementally strengthen collision avoidance controllers and C-space postural controllers ($f_c(\mathbf{q}, \dot{\mathbf{q}}) = \gamma_p(\mathbf{q}_0 - \mathbf{q}) - \gamma_d \dot{\mathbf{q}}$) to improve these performance measures in the experiment. We use the following weight scalings (first entry denotes the obstacle metric scalar, and the second entry denotes the C-space metric scalar): “low” (3, 10), “med” (5, 50), and “high” (10, 100).

Environments: We run each of these variants on 6 obstacle environments with 20 randomly sampled target locations each distributed on the opposite side of the obstacle field from the robot. Three of the environments use four smaller

obstacles (depicted in panel 3 of Fig. 5), and the remaining three environments used two large obstacles (depicted in panel 4 of Fig. 5). Each environment used the same 20 targets to avoid implicit sampling bias in target choice.

E.2 Performance measures

We report results in Fig. 4 in terms of mean and one standard deviation error bars calculated across the 120 trials for each of the following performance measures:¹³

1. *Time to goal (“time”)*: Length of time, in seconds, it takes for the robot to reach a convergence state. This convergence state is either the target, or its best-effort local minimum. If the system never converges, as in the case of many potential field trials for infeasible problems, the trial times out after 5 seconds. This metric measures time-efficiency of the movement.
2. *C-space path length (“length”)*: This is the total path length $\int \|\dot{\mathbf{q}}\| dt$ of the movement through the configuration space across the trial. This metric measures how economical the movement is. In many of the potential-field variants with lower weights, we see significant fighting among the controllers resulting in highly inefficient extraneous motions.
3. *Minimal achievable distance to goal (“goal distance”)*: Measures how close, in meters, the system is able to get to the goal with its end-effector.
4. *Percent time in collision for colliding trials (“collision intensity”)*: Given that a trial has a collision, this metric measures the fraction of time the system is in collision throughout the trial. This metric indicates the intensity of the collision. Low values indicate short grazing collisions while higher values indicate long term obstacle penetration.
5. *Fraction of trails with collisions (“collision failure”)*: Reports the fraction of trials with any collision event. We consider these to be collision-avoidance controller failures.

E.3 Discussion

In Figure 4, we see that RMPflow outperforms each of these variants significantly, with some informative trends:

1. RMPflow never collides, so its collision intensity and collision failure values are 0.
2. The other techniques, progressing from no scaling of collision-avoidance and C-space controller weights to substantial scaling, show a profile of substantial collision in the beginning to fewer (but still non-zero) collision events in the end. But we note that improvement in collision-avoidance is achieved at the expense of time-efficiency and the robot’s ability to reach the goal (it is too conservative).

¹³ There is no guarantee of feasibility in planning problems in general, so in all cases, we measure performance relative to the performance of RMPflow, which is empirically stable and near optimal across these problems.

3. Lower weight scaling of both PF-basic and PF-nonlinear actually achieve some faster times and better goal distances, but that is because the system pushes directly through obstacles, effectively “cheating” during the trial. RMPflow remains highly economical with its best effort reaching behaviors while ensuring the trials remain collision-free.
4. Lower weight scalings of PF-basic are highly uneconomical in their motion reflective of their relative instability. As the C-space weights on the posture controllers increase, the stability and economy of motion increase, but, again, at the expense of time-efficiency and optimality of the final reach.
5. There is little empirical difference between PF-basic and PF-nonlinear indicating that the defining feature separating RMPflow from the potential field techniques is its use of a highly nonlinear metric that explicitly stretches the space in the direction of the obstacle as well as in the direction of the velocity toward the target. Those stretchings penalize deviations in the stretched directions during combination with other controllers while allowing variation along orthogonal directions. By being more explicit about how controllers should instantaneously trade off with one another, RMPflow is better able to mitigate the otherwise conflicting control signals.

Summary: Isotropic metrics do not effectively convey how each collision and attractor controller should trade off with one another, resulting in a conflict of signals that obscure the intent of each controller making simultaneous collision avoidance, attraction, and posture maintenance more difficult. Increasing the weights of the controllers can improve their effectiveness, but at the expense of decreased overall system performance. The resulting motions are slower and less effective in reaching the goal in spite of more stable behavior and fewer collisions. A key feature of RMPflow is its ability to leverage highly nonlinear metrics that better convey information about how controllers should trade off with one another, while retaining provable stability guarantees. In combination, these features result in efficient and economical obstacle avoidance behavior while reaching toward targets amid clutter.

F Details of integrated system

We demonstrate the integrated vision and motion system on two physical dual arm manipulation platforms: a Baxter robot from Rethink Robotics, and a YuMi robot from ABB. Footage of our fully integrated system (see start of Section 5 for the link) depicting tasks such as pick and place amid clutter, reactive manipulation of a cabinet drawers and doors with human interaction, *active* leadthrough with collision controllers running, and pick and place into a cabinet drawer.¹⁴

¹⁴ We have also run the RMP portion of the system on an ABB IRB120 and a dual arm Kuka manipulation platform with lightweight collaborative arms. Only the two platforms mentioned here, the YuMi and the Baxter, which use the full motion and vision integration, are shown in the video for economy of space.

This full integrated system, shown in the supplementary video, uses the RMPs described in Section 3.6 (detailed in Appendix D) with a slight modification that the curvature terms are ignored. Instead, we maintain theoretical stability by using sufficient damping terms as described in Section 5.1 and by operating at slower speeds. Generalization of these RMPs between embodiments was anecdotally pretty consistent, although, as we demonstrate in our experiments, we would expect more empirical deviation at higher speeds. For these manipulation tasks, this early version of the system worked well as demonstrated in the video.

For visual perception, we leveraged consumer depth cameras along with two levels of perceptual feedback:

1. *Ambient world*: For the Baxter system we create a voxelized representation of the unmodeled ambient world, and use distance fields to focus the collision controllers on just the closest obstacle points surrounding the arms. This methodology is similar in nature to [13], except we found empirically that attending to only the closest point to a skeleton representation resulted in oscillation in concaved regions where distance functions might result in nonsmooth kinks. We mitigate this issue by finding the closest points to a *volume* around each control point, effectively smoothing over points of nondifferentiability in the distance field.
2. *Tracked objects*: We use the Dense Articulated Real-time Tracking (DART) system of [34] to track articulated objects in real time through manipulations. This system is able to track both the robot and environmental objects, such as an articulated cabinet, simultaneously to give accurate measurements of their relative configuration effectively obviating the need for explicit camera-world calibration. As long as the system is initialized in the general region of the object locations (where for the cabinet and the robot, that would mean even up to half a foot of error in translation and a similar scale of error in rotation), the DART optimizer will snap to the right configuration when turned on. DART sends information about object locations to the motion generation, and receives back information about expected joint configurations (priors) from the motion system generating a robust world representation usable in a number of practical real-world manipulation problems.

Each of our behaviors are decomposed as state machines that use visual feedback to detect transitions, including transitions to reaction states as needed to implement behavioral robustness. Each arm is represented as a separate robot for efficiency, receiving real-time information about other arm’s current state enabling coordination. Both arms are programmed simultaneously using a high level language that provides the programmer a unified view of the surrounding world and command of both arms.